

# A model for Dansgaard-Oeschger events and millennial-scale abrupt climate change without external forcing

Georg A. Gottwald

the date of receipt and acceptance should be inserted later

**Abstract** We propose a conceptual model which generates abrupt climate changes akin to Dansgaard-Oeschger events. In the model these abrupt climate changes are not triggered by external perturbations but rather emerge in a dynamic self-consistent model through complex interactions of the ocean, the atmosphere and an intermittent process. The abrupt climate changes are caused in our model by intermittencies in the sea-ice cover. The ocean is represented by a Stommel two-box model, the atmosphere by a Lorenz-84 model and the sea-ice cover by a deterministic approximation of correlated additive and multiplicative noise (CAM) process. The key dynamical ingredients of the model are given by stochastic limits of deterministic multi-scale systems and recent results in deterministic homogenisation theory. The deterministic model reproduces statistical features of actual ice-core data such as non-Gaussian  $\alpha$ -stable behaviour.

The proposed mechanism for abrupt millennial-scale climate change only relies on the existence of a quantity, which exhibits intermittent dynamics on an intermediate time scale. We consider as a particular mechanism intermittent sea-ice cover where the intermittency is generated by emergent atmospheric noise. However, other mechanisms such as freshwater influxes may also be formulated within the proposed framework.

**Keywords** Dansgaard-Oeschger events · intermittency

## 1 Introduction

A remarkable signature of the climate of the past 100 kyrs are the so called Dansgaard-Oeschger (DO) events (Dansgaard et al., 1984). These events occurred during the last glacial period and are characterised by abrupt warming within a few decades of 5-10 degrees followed by more gradual cooling over more than 1

---

School of Mathematics and Statistics  
The University of Sydney  
NSW 2006  
Australia  
E-mail: georg.gottwald@sydney.edu.au

kyr back to the stadial period with DO events recurring on a millennial time scale (Grootes and Stuiver, 1997; Yiou et al., 1997; Ditlevsen et al., 2005). They were first detected in time series of temperature proxies such as  $O^{18}$ -isotopes concentrations in ice-cores collated in Greenland (Greenland Ice-core Project (GRIP) Members, 1993; Andersen et al., 2004). The analysis of the ice-core data conveyed certain statistical features of DO events such that the abrupt warming events are consistent with non-Gaussian Lévy jump processes (so called  $\alpha$ -stable processes) (Fuhrer et al., 1993; Ditlevsen, 1999). The dynamic mechanism which gave rise to these events is still under debate. There exists a plethora of theories aimed at explaining their occurrence, ranging from conceptual models to simulations of complex coupled atmosphere-ocean general circulation models (see the excellent reviews by Crucifix (2012) and by Li and Born (2019)). Most theories are built around the premise that the ocean is the main agent controlling the DO events, and that the ocean’s meridional overturning circulation (MOC) is reduced by freshwater influx (Manabe and Stouffer, 2011; Friedrich et al., 2010). This hypothesis has been tested in ocean general circulation models by studying the ocean response to prescribed freshwater flushes (Weaver and Hughes, 1994; Ganopolski and Rahmstorf, 2001; Haarsma et al., 2001; Meissner et al., 2008; Timmermann et al., 2003). How these freshwater fluxes were produced in the first place is, however, left out in these studies. There is a need to develop a self-consistent mechanism for DO events, which does not rely on external factors not covered by the model. Moreover, the pivotal role of internal ocean dynamics has been questioned by Wunsch (2006). Therein it is argued that the ocean’s net meridional heat transport is not sufficiently strong to cause the massive changes in temperature as suggested from the ice-core data, and that “the oceanic tail may not necessarily be wagging the meteorological dog”. It has instead been recognised recently that DO events involve an intimate and complex interaction between the ocean, sea-ice and the atmosphere (see the comprehensive review by Li and Born (2019)). In particular the role of stochastic wind forcing (Monahan et al., 2008; Drijfhout et al., 2013; Kleppin et al., 2015), the importance of sea-ice and its changes (Gildor and Tziperman, 2003; Li et al., 2005; Petersen et al., 2013; Dokken et al., 2013; Zhang et al., 2014; Kleppin et al., 2015; Hoff et al., 2016; Boers et al., 2018; Sadatzki et al., 2019), the vertical structure of the Nordic seas (Singh et al., 2014; Jensen et al., 2016) as well as inter-hemisphere coupling mediated by Southern Ocean winds (Banderas et al., 2012, 2015) have all been found to have a significant effect on the phenomenon of DO events.

Building on these current developments in our understanding of DO events, we develop here a conceptual model for millennial-scale abrupt climate change consisting of a coupled dynamical system modelling the interactions between the ocean, sea-ice and the atmosphere, without any external forcing such as prescribed freshwater fluxes. We do so in an entirely deterministic fashion. The importance of stochastic atmospheric dynamics (Monahan et al., 2008; Drijfhout et al., 2013; Dokken et al., 2013; Kleppin et al., 2015) and the observed effective  $\alpha$ -stable statistics of the ocean temperature (Ditlevsen, 1999) are accounted for via deterministically self-generated noise in a multi-scale setting. On the slow scale the ocean is modelled by a Stommel two-box model (Stommel, 1961) which is forced by an intermittent sea-ice model on an intermediate time scale. The atmosphere enters the model in form of a Lorenz-84 model on the fastest time scale, modelling

80 jet streams and baroclinic eddy activity (Lorenz, 1984). We consider here the possi-  
81 bility of two atmospheric Lorenz-84 models, one for the Northern hemisphere  
82 and one for the Southern hemisphere (Banderas et al., 2012, 2015). The strongly  
83 chaotic atmosphere gives rise to Gaussian noise on the slower time scales of the  
84 sea-ice and of the ocean. The crucial premise of our model is that sea-ice is inter-  
85 mittent and that its dynamics is punctuated by sporadic events of extreme large  
86 sea-ice cover. The effect of atmospheric forcing on the variations of sea-ice has long  
87 been recognised (Fang and Wallace, 1994; Venegas and Mysak, 2000; Deser et al.,  
88 2002). In our model chaotic weather dynamics deterministically generates intermit-  
89 tent sea-ice dynamics. The emerging weakly chaotic intermittent sea-ice dynamics  
90 then subsequently generates the necessary non-Gaussian Lévy noise in the slow  
91 ocean dynamics, driving the ocean temperature abruptly from its glacial steady  
92 (noisy) state to a warmer unstable state.

93 From a dynamical systems point of view the theoretical backbone of the model  
94 consists of statistical limit laws to generate stochastic processes by appropriately  
95 integrating deterministic chaotic dynamics and hinges on recent advances in the  
96 study of diffusive limits of deterministic multi-scale systems (Melbourne and Stuart,  
97 2011; Gottwald and Melbourne, 2013b; Kelly and Melbourne, 2016; Chevyrev et al.,  
98 2019). Therein it is shown that noise can be deterministically generated within a  
99 multi-scale system. If the driving fast process is *strongly* chaotic, the slow dynam-  
100 ics is, in the limit of infinite time-scale separation, in effect a stochastic differ-  
101 ential equation driven by Brownian (possibly multiplicative) noise. The mecha-  
102 nism can be motivated heuristically as follow: within one slow time unit the slow  
103 dynamics integrates the chaotic fast process and, invoking a central limit type  
104 argument, one ends up with an effective Gaussian noise. However, as was shown  
105 by Ditlevsen (1999), ice-core data exhibit a strong degree of non-Gaussian  $\alpha$ -  
106 stable dynamics. Anomalous  $\alpha$ -stable noise, or a Lévy process, is characterised  
107 by jumps at all scales with non-zero probability of large jumps (see, for ex-  
108 ample, Chechkin et al. (2008) for an exposition of  $\alpha$ -stable processes). As for  
109 the Gaussian noise discussed above,  $\alpha$ -stable Lévy noise can be deterministi-  
110 cally generated in an entirely deterministic fashion. The deterministic origin of  
111 anomalous diffusion can be linked to intermittent fast dynamics in which the  
112 dynamics spends long temporal intervals near a marginally stable fixed point  
113 or periodic orbit before experiencing chaotic bursts (Gaspard and Wang, 1988).  
114 The central limit theorem which generated the Gaussian noise in the case of  
115 strongly chaotic non-intermittent dynamics ceases to be valid but can be re-  
116 placed by a modified statistical law (Gouëzel, 2004). Gottwald and Melbourne  
117 (2013b); Chevyrev et al. (2019) showed that for multi-scale systems with a weakly  
118 chaotic intermittent fast driving process the limiting stochastic process of the slow  
119 dynamics is given by (possibly multiplicative)  $\alpha$ -stable noise<sup>1</sup> We consider here  
120 intermittent sea-ice dynamics modelled by correlated additive and multiplica-  
121 tive noise (CAM) (Sura and Sardeshmukh, 2008; Sardeshmukh and Sura, 2009;  
122 Penland and Sardeshmukh, 2012; Sardeshmukh and Penland, 2015). CAM noise  
123 naturally arises in deterministic multi-scale systems for the effective slow dynam-  
124 ics (Sardeshmukh and Sura, 2009; Majda et al., 2009). Using statistical limit laws  
125 developed by Kuske and Keller (2001), Thompson et al. (2017) showed that fast

---

<sup>1</sup> See Gottwald and Melbourne (2013a) for a definition of what constitutes strong and weak chaos.

intermittent CAM noise can be used to generate  $\alpha$ -stable processes. Within the framework of statistical limit laws we can now highlight the dynamic function of the geophysical ingredients of our coupled ocean-atmosphere sea-ice model: using the classical central limit theorem, a fast atmospheric model generates intermittent Brownian CAM noise of the sea-ice dynamics on an intermediate time scale. The sea-ice dynamics then generates  $\alpha$ -stable noise on the slow oceanic time scale by means of a generalised central limit theorem. We show that the emerging stochastic dynamics of this coupled ocean-atmosphere and sea-ice model is able to generate abrupt changes in the temperature akin of DO events.

The paper is organised as follow. In Section 2 we perform an analysis of ice-core data confirming that the data are consistent with a dynamic process involving  $\alpha$ -stable noise. Section 3 provides a heuristic approach to deterministic generation of stochastic processes, covering both the Gaussian and the  $\alpha$ -stable case. Sections 4 and 5 are the heart of the paper. Section 4 introduces the deterministic coupled ocean-atmosphere and sea-ice model. Section 5 provides numerical simulations illustrating the capability of the model to capture abrupt climate changes akin to DO events. We conclude in Section 6 with a discussion.

## 2 Time series analysis of ice-core data

Ice core data have immensely increased our knowledge about past climate variations (Greenland Ice-core Project (GRIP) Members, 1993; Andersen et al., 2004). An analysis of calcium ice core data collated in central Greenland as part of the GRIP programme (Fuhrer et al., 1993) was performed by Ditlevsen (1999). Calcium originates from dust deposited on the ice and is not diffusing as much as the usual  $\delta^{18}\text{O}$  proxy allowing for a higher temporal resolution. The logarithm of the calcium concentration is negatively correlated with  $\delta^{18}\text{O}$ , with higher concentrations of  $\text{Ca}^{2+}$  in colder conditions due to enhanced exposure to sea shelves caused by lower sea levels, increased aridity and stronger zonal winds caused by an increased meridional temperature gradient (Fuhrer et al., 1993; Schüpbach et al., 2018). The time series of  $-\log(\text{Ca})$  is shown in Figure 1 together with the time series of  $\delta^{18}\text{O}$  illustrating their strong correlation. The data for  $\delta^{18}\text{O}$  were obtained from the NGRIP programme using the Greenland Ice Core Chronology (GICC05) time scale and the GICCO05modelext time scale for times past 60kyr before year 2000 (Vinther et al., 2006; Rasmussen et al., 2006; Andersen et al., 2006; Svensson et al., 2008; Wolff et al., 2010). The time series of  $\log(\text{Ca})$  exhibits strong non-Gaussian character. Ditlevsen (1999) found that the data contain a significant  $\alpha$ -stable component with a stability parameter  $\alpha = 1.75$  in conjunction with multiplicative Gaussian noise.

We briefly revisit the analysis, using a different method to detect the  $\alpha$ -stable component. We assume that the data can be modelled by a one-dimensional stochastic differential equation of the form  $dX = -U'(X)dt + \sigma_w dW_t + dL_\alpha$  where  $W_t$  is standard Brownian motion and  $L_\alpha$  is an  $\alpha$ -stable stochastic process. The prime denotes the derivative with respect to  $X$ . The potential  $U(X)$  can be readily estimated from the data by using standard coarse graining of the data to estimate the conditional average of  $dX$  (Gardiner, 2003; Siegert et al., 1998; Stemler et al.,

2007). We obtain a quartic potential  $U(X) = 0.0018 X^4 - 0.0058 X^3 + 0.0024 X^2 + 0.0028 X$  where the two potential well minima correspond to the stadial and interstadial regimes (see also Kwasiński and Lohmann (2009); Lohmann and Ditlevsen (2019)). The colder potential minimum is more stable than the warmer one. To estimate the presence of  $\alpha$ -stable noise we will not, as in Ditlevsen (1999), study the scaling of the tails of the empirical probability density function (which scales as  $X^{-\alpha-1}$ ), but rather employ the method of  $p$ -variation (Magdziarz et al., 2009; Magdziarz and Klafter, 2010; Hein et al., 2009). Whereas the presence of fat tails may also be caused by multiplicative Gaussian noise,  $p$ -variation is a proper statistics to isolate  $\alpha$ -stable behaviour. The statistics concerns the asymptotic behaviour of

$$V_p^n(t) = \sum_{k=1}^{\lfloor nt \rfloor} |X(k/n) - X((k-1)/n)|^p.$$

165 This easily computable statistics measures the roughness of the process  $X$ , tun-  
 166 ing into finer and finer partitions with increasing  $n$ . For  $p = 1$  the statistics re-  
 167 duces to the total variation and for  $p = 2$  it reduces to the quadratic variation.  
 168 For Brownian motion where increments scale as  $\sqrt{1/n}$  one obtains in the limit  
 169 of  $n \rightarrow \infty$  that  $V_2^n(t) \sim t$ , and  $V_p^n(t) \rightarrow 0$  for  $p > 2$ . Given an  $\alpha$ -stable pro-  
 170 cess  $X$  for some  $\alpha < 2$ , the statistics  $V_p^n(t)$  converges for  $p > \alpha$  and diverges  
 171 for  $p < \alpha$ . In Hein et al. (2009) it was shown that if  $X$  is a stochastic pro-  
 172 cess  $dX = -U'(X)dt + \sigma_w dW_t + dL_\alpha$  driven by  $\alpha$ -stable noise with  $\alpha = p/2$   
 173 then  $V_p^n(t)$  converges in distribution to  $L_{1/2}$ . This suggests to use a Kolmogorov-  
 174 Smirnov test and find the value of  $p = 2\alpha$  for which the empirical cumulative  
 175 distribution function is closest to the target cumulative distribution function of  
 176  $L_{1/2}$ . To estimate the cumulative distribution function we follow Hein et al. (2009)  
 177 and choose to divide the Ca time series into 282 segments, each consisting of 282  
 178 data points. The minimal Kolmogorov-Smirnov distance is then found by varying  
 179 the scale parameter of the target distribution  $L_{1/2}$  for each value of  $p$ . The value  
 180  $p^*$  for which the minimum is attained then determines  $\alpha = p^*/2$ . For details on  
 181 the  $p$ -variation method see (Magdziarz et al., 2009; Magdziarz and Klafter, 2010;  
 182 Hein et al., 2009). We remark that Hein et al. (2009) found a value of  $\alpha = 0.75$ ,  
 183 suggesting a Lévy process with infinite mean. We find here, in reasonably close  
 184 agreement with the result by Ditlevsen (1999), the value of  $\alpha = 1.78$ . In our model,  
 185 introduced in Section 4, the particular feature of DO events to exhibit  $\alpha$ -stable  
 186 statistics will be generated by intermittent sea-ice dynamics.

### 187 3 Dynamic mechanism to generate Brownian motion and Lévy noise 188 from deterministic multi-scale systems

The model developed in Section 4 relies on recent developments in the study of stochastic limits of deterministic multi-scale systems. The mathematical programme to derive limiting stochastic slow dynamics is coined homogenisation (Givon et al., 2004). The machinery of homogenisation provides explicit expressions for the drift and diffusion components of the effective stochastic slow dynamics. In particular, we will use results from deterministic homogenisation of multi-scale systems (Melbourne and Stuart, 2011; Gottwald and Melbourne, 2013b; Kelly and Melbourne,

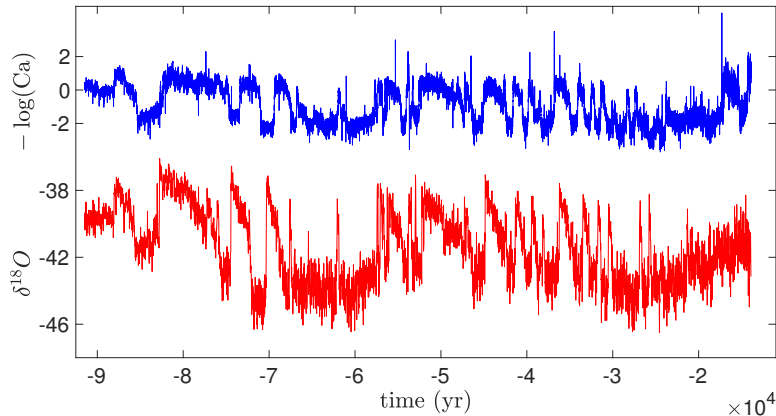


**Fig. 1** The negative logarithm of the calcium concentration and  $\delta^{18}\text{O}$  as a function of time. The Ca time series was obtained from the GRIP ice-core data and have a temporal resolution of approximately 1 year, and there are a total of 79,957 data points between 11 kyrs and 91 kyrs. The  $\delta^{18}\text{O}$  time series was obtained from NGRIP ice-core data and have a temporal resolution of 20 years with 6,114 data points.

2017; Chevyrev et al., 2019). Rather than stating the theorems we present here, following Gottwald et al. (2017), a heuristic motivation to illustrate how deterministic multi-scale systems can give rise to an effective stochastic dynamics for the slow variables. Consider the slow-fast system for slow variables  $x_\varepsilon$  and fast variables  $y_\varepsilon$

$$\dot{x}_\varepsilon = \varepsilon^{\gamma-1} h(x_\varepsilon) f(y_\varepsilon), \quad x_\varepsilon(0) = x_0 \quad (1)$$

$$\dot{y}_\varepsilon = \varepsilon^{-1} g(y_\varepsilon), \quad y_\varepsilon(0) = y_0, \quad (2)$$

which is formulated on the fast time scale. Here  $\varepsilon \ll 1$  denotes the time scale separation and  $\gamma \geq \frac{1}{2}$ . We assume that the fast dynamics is supported on a chaotic attractor and is statistically stationary in the sense that averages can be computed by means of temporal averages. Integration of the slow dynamics yields

$$x_\varepsilon(t) = x_0 + \varepsilon^\gamma \int_0^{\frac{t}{\varepsilon}} h(x_\varepsilon(\tau)) f(y_\varepsilon(\tau)) d\tau.$$

Introducing  $n = \varepsilon^{-1}$  and  $\alpha = 1/\gamma$  we obtain

$$x_\varepsilon(t) = x_0 + \frac{1}{n^\alpha} \int_0^{tn} h(x_\varepsilon(\tau)) f(y_\varepsilon(\tau)) d\tau. \quad (3)$$

Consider first the case  $\alpha = \gamma = 1$ , then for  $n \rightarrow \infty$  (or equivalently for  $\varepsilon \rightarrow 0$ ) the temporal integral is simply the average over the fast dynamics, and by the law of large numbers (the most simple statistical limit law) the slow dynamics remains deterministic in the limit  $\varepsilon \rightarrow 0$ , and solutions  $x_\varepsilon(t)$  converge to solutions of the deterministic equation  $\dot{X} = Fh(X)$  with  $X(0) = x_0$  where  $F \equiv \text{const}$  is the average over the fast dynamics of  $f(y_\varepsilon)$ . Now consider the case when the average is zero with  $F \equiv 0$ . Clearly, the implied deterministic limit  $X(t) = X(0)$  does not

capture the dynamics of the solution  $x_\varepsilon(t)$  of the actual multi-scale system which is constantly driven by non-zero  $f(y_\varepsilon(t))$ . One needs to go to longer time scales to see these fluctuations sum up to generate noise. This can be seen from (3) by setting  $\alpha = 2$  (i.e.  $\gamma = \frac{1}{2}$ ). For  $\alpha = 2$  the integral is reminiscent of the central limit theorem. Indeed using statistical limit laws for strongly chaotic dynamical systems (Melbourne and Nicol, 2005, 2009), the integral term converges to Gaussian noise. For the purpose of this exposition it is sufficient to think of *strongly* chaotic dynamical systems as systems for which the auto-correlation function is integrable; this will be contrasted to *weakly* chaotic dynamical systems for which the auto-correlation function is not integrable (Gottwald and Melbourne, 2013a). It is important to note that it is not the chaotic signal  $y_\varepsilon$  itself that is noisy but rather the integrated fast chaotic variable. Care has to be taken in what way the stochastic integral in (3) is to be interpreted (Gottwald and Melbourne, 2013b; Kelly and Melbourne, 2017). In the case of 1-dimensional slow variables  $x_\varepsilon$ , which will be considered in Section 4 for the sea-ice model, the stochastic integrals are in the sense of Stratonovich, i.e. classical calculus is preserved in the limiting process when passing from the smooth deterministic multi-scale system to the rough stochastic differential equation. In this case, the slow dynamics of the multi-scale system (1)–(2) converges on the slow times  $x_\varepsilon(t/\varepsilon) \rightarrow X(t)$  where  $X$  satisfies the stochastic differential equation

$$dX = \Sigma h(X) \circ dW_t, \quad (4)$$

with standard Brownian motion  $W_t$  (and  $\circ$  denoting that the noise is to be interpreted in the sense of Stratonovich) and the diffusion coefficient is given by the Green-Kubo formula

$$\Sigma = \int_0^\infty C(t) dt,$$

with normalised auto-correlation

$$C(t) = \frac{1}{\sigma^2} \int_0^\infty f_0(y_\varepsilon(t+s)) f_0(y_\varepsilon(s)) ds$$

189 with  $C(0) = 1$ . The diffusion coefficient  $\Sigma$  is well defined if the auto-correlation  
190 function is integrable.

There is, however, a class of weakly chaotic dynamical systems, for which the central limit theorem breaks down and fluctuations are of the Lévy type rather than Gaussian. Weakly chaotic dynamics is characterised by intermittent behaviour where the dynamics spends extensive time near “sticky” equilibria or periodic orbits before sporadic excursive bursts away from those marginally unstable objects. It has recently been shown that, if  $f(y_\varepsilon)$  is non-zero in the laminar phase, the central limit theorem can be replaced for weakly chaotic dynamics and the integral term in (3) converges in distribution to a stable law  $L_{\alpha,\eta,\beta}$  of exponent  $\alpha \in (1, 2)$  (Gouëzel, 2004). The stability parameter  $\alpha$  determines the algebraic decay in the tail of the probability density function, the scale parameter  $\eta$  measures the spread of the distribution around its maximum and the skewness parameter  $\beta$  encapsulates the probability of the process experiencing a positive jump or negative jump with  $\beta = \pm 1$  having only positive/negative jumps. Gottwald and Melbourne

(2013b); Chevyrev et al. (2019) showed that for intermittent fast dynamics (2) solutions  $x_\varepsilon$  converge weakly to solutions of the stochastic differential equation

$$dX = h(X) \diamond dL_{\alpha,\eta,\beta}, \quad X(0) = x_0. \quad (5)$$

The parameters  $\alpha$ ,  $\beta$  and  $\eta$  of the Lévy process  $L_{\alpha,\eta,\beta}$  are determined by the statistical properties of the driver  $f(y_\varepsilon)$ . The diamond denotes that the noise  $h(X) \diamond dL$  is to be interpreted in the sense of Marcus (Marcus, 1981; Applebaum, 2009; Chechkin and Pavlyukevich, 2014). The Marcus interpretation is the analogue of the Stratonovich interpretation for Brownian noise in the sense that classical calculus prevails, consistent with the intuition that one expects that the noise arises as a limit involving only smooth functions of a smooth deterministic system, and hence classical calculus should be inherited by the limiting system. We remark that the noise is of Marcus type independent of the dimension of the slow variables, unlike for the Stratonovich interpretation in the case of Brownian motion which is only ensured for 1-dimensional slow variables. The Marcus integral  $\int^t h(X) \diamond dL_{\alpha,\eta,\beta}(s)$  involves cumbersome expressions such as sums over infinitely many jumps. Moreover, whereas one can pass readily between the Stratonovich integrals to Itô integrals, this is not possible for Marcus integrals. In our applications here, however, the  $\alpha$ -stable noise will be additive and these issues do not arise. The convergence to a Lévy process can be heuristically understood by realising that if the dynamics  $y_\varepsilon$  is near the marginally unstable fixed point  $y_\varepsilon = y_\varepsilon^*$ , the slow dynamics is driven by a constant  $h(x_\varepsilon)f(y_\varepsilon^*)$  (note that on the fast time scale  $\tau = t/\varepsilon$   $x_\varepsilon$  is approximately constant). Hence the slow variable experiences ballistic drift during the laminar phases. It is those long ballistic drifts which amount to the jumps of the Lévy process when viewed on a long time scale (see Gottwald and Melbourne (2013a, 2016, 2020) for numerical illustrations of this mechanism).

In a different strand of work, based on statistical limit laws for stochastic dynamical systems (Kuske and Keller, 2001), Thompson et al. (2017) argue that so called correlated additive and multiplicative (CAM) noise processes

$$dy_\varepsilon = Ly_\varepsilon dt - \frac{E}{2}G dt + (Ey_\varepsilon + G) \circ dW_1 + B dW_2 \quad (6)$$

with independent standard Brownian motions  $W_{1,2}$  and  $L < 0$  lie in the domain of  $\alpha$ -stable processes which means that they give rise to  $\alpha$ -stable processes when integrated. For  $B \neq 0$  the mean is well defined and one has explicit expressions for the parameters of the resulting Lévy process  $\alpha$ ,  $\beta$  and  $\eta$  as functions of the parameters of the CAM process (Kuske and Keller, 2001; Thompson et al., 2017). The stability parameter  $\alpha$  of the resulting  $\alpha$ -stable process  $L_{\alpha,\eta,\beta}$  is given by

$$\alpha = -2\frac{L}{E^2}, \quad (7)$$

the skewness parameter is given by

$$\beta = \tanh\left(\frac{\pi G(\alpha - 1)}{2B}\right) \quad (8)$$

and the scale parameter  $\eta$  is given by

$$\eta = \left( \frac{2 \cosh\left(\frac{\pi G(\alpha - 1)}{2B}\right)}{E^{\alpha+1} \alpha N} \Gamma(1 - \alpha) \cos\left(\frac{\pi}{2}\alpha\right) \right)^{\frac{1}{\alpha}}$$



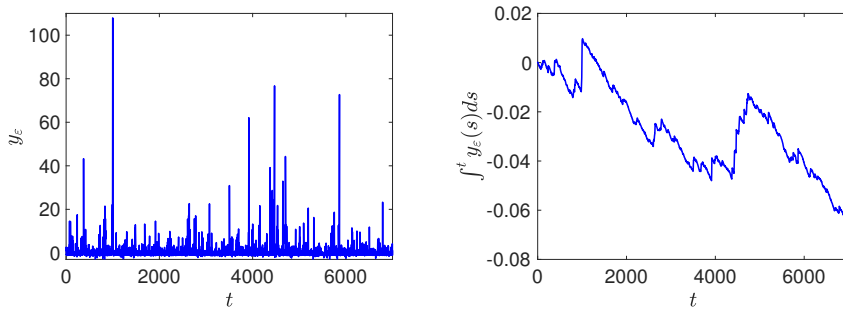


**Fig. 2** Left: Realisation of a CAM process with  $(L, E, G, B) = (-0.94, 1.118, 1, 0.3)$ . Right: Approximation of an  $\alpha$ -stable process with  $\alpha = 1.5$  and  $\beta = 0.99$  from the time series shown on the left.

with

$$N = 2\pi(2B)^{-\alpha} \frac{\Gamma(\alpha)}{E\Gamma(z)\Gamma(\bar{z})}, \quad z = \frac{\alpha + 1}{2} + i \frac{G(\alpha - 1)}{B},$$

213 where the bar denotes the complex conjugate.

214 Figure 2 shows an example of a time series of a CAM process with  $L = -0.94$ ,  
 215  $E = 1.118$ ,  $G = 1$  and  $B = 0.3$ , implying that  $\xi = \varepsilon^\gamma \int^{t/\varepsilon} f(y_\varepsilon(s)) ds$  with  $\gamma = 1/\alpha$   
 216 converges to an  $\alpha$ -stable process with  $\alpha = 1.5$  and  $\beta = 0.99$  (implying that there  
 217 are almost only upwards jumps). Here the mechanism of generating  $\alpha$ -stable noise  
 218 is different to the one described above: rather than the jumps consisting of many  
 219 small jumps during the long laminar phases of varying length, the jumps here are  
 220 caused by the sporadic peaks of varying sizes.

221

222 In Section 4 we shall model sea-ice by a deterministic approximation of a CAM  
 223 process, whereby the two independent Brownian motions  $W_{1,2}$  are approximated  
 224 by two uncorrelated fast strongly chaotic processes, along the lines described above.

#### 225 4 Coupled ocean-atmosphere and sea-ice model

We construct a conceptual deterministic coupled ocean-atmosphere and sea-ice model. The ocean model is given by a Stommel two-box model (Stommel, 1961) and the atmosphere is represented by a Lorenz-84 model, describing the westerly jet stream and large-scale eddies (Lorenz, 1984). The sea-ice is modelled by a linear intermittent CAM process driven by the fast atmosphere and is characterised by sporadic brief periods of large sea-ice extent (cf. Figure 2). The intermittent character of the sea-ice is the main premise of our model and is paramount to generate the abrupt climate changes of DO events. The abrupt climate changes are a signature of an emerging  $\alpha$ -stable driving signal induced by integrated intermittent sea-ice dynamics. To deterministically generate the  $\alpha$ -stable noise on the slow oceanic time scale using the statistical limit theorems outlined in Section 3, two further scales are required besides the slow oceanic time scale: a fast and an intermediate time scale. The fast strongly chaotic atmosphere dynamics integrates on the intermediate time scale of the sea-ice to Brownian motion to generate CAM

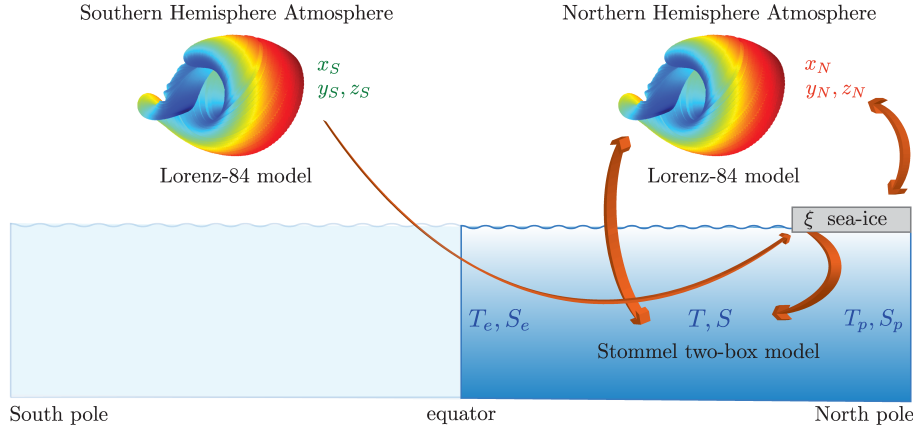


**Fig. 3** Schematic of the coupled ocean-atmosphere and sea-ice model, highlighting the interdependencies and the characterising variables.

noise. Then the CAM noise is integrated on the slow oceanic time scale to generate  $\alpha$ -stable Lévy noise. We impose the natural time scale separation of the slow ocean with the typical diffusive time scale estimated as 219 years (Cessi, 1994), an intermediate sea-ice dynamics occurring on time scales of months and a fast atmosphere with typical time scales of days. This suggest to introduce time scale parameters for the fast atmosphere  $\epsilon_f$  and the intermediate sea-ice dynamics  $\epsilon_i$  as

$$\epsilon_f = \frac{1}{365 \times 219} \approx 1.25 \times 10^{-5}, \quad (9)$$

$$\epsilon_i = \frac{30}{365 \times 219} \approx 3.75 \times 10^{-4}. \quad (10)$$

The ocean is characterised by coarse meridional temperature and salinity gradients

$$T = T_e - T_p, \quad (11)$$

$$S = S_e - S_p, \quad (12)$$

226 where the subscripts  $e$  and  $p$  denote the respective values at equatorial and polar  
 227 locations. The sea-ice dynamics is characterised by the extent of the sea-ice cover  
 228  $\xi$ . The atmosphere is characterised by the westerly zonal mean flow  $x_{N,S}$  and the  
 229 superimposed large scale eddies with amplitudes  $y_{N,S}$  and  $z_{N,S}$ . Subscripts  $N$  and  
 230  $H$  denote the respective values of the Northern and Southern hemisphere. We first  
 231 present the coupled non-dimensional model (13)–(18) for these variables together  
 232 with the coupling terms (19)–(22) capturing the various interactions between the  
 233 ocean, atmosphere and sea-ice, before deriving the model and the non-standard  
 234 coupling terms in Sections 4.1–4.3. Figure 3 presents a schematic illustrating the  
 235 model and its various dependencies. For ease of navigation relevant variables and  
 236 parameters are listed in Table 1.

Specifically, we propose the following model: the ocean is described by a Stommel two-box model

$$\dot{T} = -\frac{1}{\epsilon_a} (T - \Theta(t)) - T - \mu|S - T|T - \frac{1}{\epsilon_i^{1-\gamma}} d(\xi - \bar{\xi})T \quad (13)$$

$$\dot{S} = \sigma(t) - S - \mu|S - T|S, \quad (14)$$

Variable/Parameter	Brief description
<b>fast atmosphere: Lorenz-84 model</b>	
(for Northern (H) and Southern (S) hemisphere)	
$x_{N,S}$	strength of westerly zonal mean flow
$y_{N,S}, z_{N,S}$	amplitude of sine and cosine phase of large-scale eddy
$\Delta_{N,S}$	eddy energy with $\Delta = y^2 + z^2$
$F^{N,S}$	meridional temperature gradient
$G^{N,S}$	longitudinal temperature gradient
<b>intermediate sea-ice model: CAM noise</b>	
$\xi$	sea-ice cover
<b>slow ocean: Stommel two-box model</b>	
$T$	temperature gradient $T = T_e - T_p$ between equatorial and polar ocean
$S$	salinity gradient $S = S_e - S_p$ between equatorial and polar ocean
$\Theta$	ambient temperature gradient
$\sigma$	freshwater flux
<b>global coupling parameters</b>	
$\epsilon_f$	ratio of characteristic time scales of fast atmosphere and slow ocean
$\epsilon_i$	ratio of characteristic time scales of intermediate sea-ice and slow ocean
$\gamma$	inverse of stability parameter of the $\alpha$ -stable process with $\gamma = 1/\alpha$

**Table 1** Variables and parameters used for the coupled ocean-atmosphere and sea-ice model.

where  $\epsilon_a$  measures the relaxation of the ocean temperature to the ambient temperature  $\Theta(t)$ ,  $\mu$  quantifies the transport strength and  $\sigma(t)$  denotes freshwater flux. A more detailed definition of the parameters is provided in Section 4.1. The parameter  $\gamma$  controls the application of the statistical limit theorems discussed in Section 3 to generate Lévy noise with stability parameter  $\alpha = 1/\gamma$ . The ocean-dynamics couples to the sea-ice dynamics

$$\epsilon_i \dot{\xi} = \left(\lambda + \frac{\kappa^2}{2}\right)\xi + \sqrt{\frac{\epsilon_i}{\epsilon_f}} \delta(\kappa\xi + g)(x_S - \bar{x}_S) + \sqrt{\frac{\epsilon_i}{\epsilon_f}} c(\Delta_N - \bar{\Delta}_N), \quad (15)$$

where the sea-ice dynamics is driven by the Northern hemisphere atmosphere through the eddy strength  $\Delta_N = y_N^2 + z_N^2$  and by the Southern hemisphere atmosphere by the jet stream  $x_S$ . The parameters  $\lambda, \kappa, \delta, g, c$  allow for tuning of the  $\alpha$ -stable noise emerging in the ocean model (13) (cf. (6)). The atmospheres of the Northern and Southern hemisphere are modelled by two Lorenz-84 systems

$$\epsilon_f \dot{x}_{N,S} = -(y_{N,S}^2 + z_{N,S}^2) - a^{(N,S)}(x_{N,S} - F^{(N,S)}) \quad (16)$$

$$\epsilon_f \dot{y}_{N,S} = x_{N,S} y_{N,S} - b^{(N,S)} x_{N,S} z_{N,S} - (y_{N,S} - G^{(N,S)}) \quad (17)$$

$$\epsilon_f \dot{z}_{N,S} = b^{(N,S)} x_{N,S} y_{N,S} + x_{N,S} z_{N,S} - z_{N,S}. \quad (18)$$

To generate Brownian motion in the sea-ice dynamics (15) the only requirement for the choice of the parameters  $a^{(N,S)}$ ,  $b^{(N,S)}$ ,  $F^{(N,S)}$  and  $G^{(N,S)}$  is that the

Lorenz-84 systems supports chaotic dynamics. The southern meridional and longitudinal temperature gradients  $F^{(S)}$  and  $G^{(S)}$  are set to constant  $F^{(S)} = F_0^{(S)}$  and  $G^{(S)} = G_0^{(S)}$  whereas the northern meridional and longitudinal temperature gradients  $F^{(N)}$  and  $G^{(N)}$  include back-coupling to the ocean dynamics and the sea-ice via

$$F^{(N)} = F_0^{(N)} + F_1^{(N)}T + F_2^{(N)}\xi \quad (19)$$

$$G^{(N)} = G_0^{(N)} - G_1^{(N)}T - G_2^{(N)}\xi, \quad (20)$$

with  $F_{1,2}^{(N)} \geq 0$  and  $G_{1,2}^{(N)} \geq 0$ . The ambient temperature gradient  $\Theta(t)$  of the ocean is driven by the atmosphere via thermal wind balance and is modelled as

$$\Theta(t) = \theta_0 + \theta_1 \frac{x_N - \bar{x}_N}{\sqrt{\epsilon_f}}, \quad (21)$$

and the salinity gradient  $S$  is driven by the freshwater flux  $\sigma(t)$  which is affected by both the atmosphere and the sea-ice, and is modelled as

$$\sigma(t) = \sigma_0 + \sigma_1 \frac{\Delta_N - \bar{\Delta}_N}{\sqrt{\epsilon_f}} + \sigma_2 \frac{\dot{\xi} - \bar{\xi}}{\epsilon_i^{1-\gamma_\xi}}. \quad (22)$$

237 The model (13)–(18) includes a wide range of interactions between the ocean,  
 238 the atmosphere and the sea-ice, captured in (19)–(22). To obtain abrupt warming  
 239 events, however, it is sufficient to consider a minimal model with  $F_1^{(N)} = F_2^{(N)} =$   
 240  $G_1^{(N)} = G_2^{(N)} = \theta_1 = \sigma_1 = \sigma_2 \equiv 0$ . To reproduce realistic stochastic variations,  
 241 however, we include atmospheric noise on the ocean dynamics and allow for  $\theta_1 \neq 0$   
 242 and  $\sigma_1 \neq 0$  in the numerical simulations presented in Section 5.

243

244 We derive the model (13)–(18) with its coupling terms (19)–(22) in the follow-  
 245 ing subsections. We begin by first deriving the classical Stommel two-box model on  
 246 the slow time scale. We then continue setting up the atmosphere dynamics on the  
 247 fastest time scale with a Lorenz-84 model and discuss how the atmosphere and the  
 248 ocean couple. Finally, we set out to propose our model for the intermittent sea-ice  
 249 dynamics and discuss how it modifies the dynamics of the (northern) atmosphere  
 250 and ocean.

#### 251 4.1 Ocean model

We first formulate the ocean model on the slow time scale. We consider here the Stommel two-box model for the temperatures  $T_{e,p}$  and salinities  $S_{e,p}$  of an equatorial ocean box and a polar ocean box, respectively, (Stommel, 1961). Although the derivation is standard and the box model is part of the canonical suite of conceptual models we present the derivation to illustrate the order of magnitude of the respective parameters of our model. We follow here Cessi (1994) and Roebber

(1995) in the derivation. From conservation of heat, salt and water mass one obtains

$$\begin{aligned}\dot{T}_e &= -\frac{1}{t_r} (T_e - \Theta_e(t)) - \frac{1}{2}\Psi(\Delta\rho) (T_e - T_p) \\ \dot{T}_p &= -\frac{1}{t_r} (T_p + \Theta_p(t)) - \frac{1}{2}\Psi(\Delta\rho) (T_p - T_e) \\ \dot{S}_e &= \frac{W_e(t)}{H} - \frac{1}{2}\Psi(\Delta\rho) (S_e - S_p) \\ \dot{S}_p &= -\frac{W_p(t)}{H} - \frac{1}{2}\Psi(\Delta\rho) (S_p - S_e).\end{aligned}$$

Here  $\Theta_{e,p}(t)$  are the ambient atmospheric temperatures the ocean would equilibrate to on a relaxation time  $t_r$  without any mass and heat exchange. The flux  $\Psi(\Delta\rho)$ , capturing the mass and heat exchange, is driven by the density difference  $\Delta\rho = \rho_e - \rho_p$  between the two ocean boxes. The densities are assumed to be linearly related to the temperature and salinity with  $\rho_{e,p}/\rho_0 = 1 + \alpha_s(S_{e,p} - S_0) - \alpha_T(T_{e,p} - T_0)$ . The functions  $W_{e,p}$ , scaled with the typical height of the boxes  $H$ , model salinity sources or sinks  $W_{\text{precept}}$  associated with precipitation/evaporation and/or freshwater sources  $W_{\text{fresh}}$  stemming from melting land ice. (Note that with slight abuse of notation, we use  $W$  in this section to denote the salinity sinks and sources, and use  $W$  otherwise to denote Brownian motion). We set  $W_e(t) = W_{\text{prec}}(t)/2$  and  $W_p(t) = W_{\text{prec}}(t)/2 + W_{\text{fresh}}(t)$ . Introducing the coarse meridional temperature and salinity gradients  $T = T_e - T_p$  and  $S = S_e - S_p$  we obtain

$$\dot{T} = -\frac{1}{t_r} (T - \Theta(t)) - \Psi(\Delta\rho)T \quad (23)$$

$$\dot{S} = \frac{W_e(t) + W_p(t)}{H} - \Psi(\Delta\rho)S, \quad (24)$$

with  $\Theta(t) = \Theta_e(t) - \Theta_p(t)$ . Following Stommel (1961) the flux is assumed to involve a diffusive component on the diffusive time scale  $t_d$  and a hydraulic component of a Poiseuille flow with transport coefficient  $q$ , and we write

$$\begin{aligned}\Psi(\Delta\rho) &= \frac{1}{t_d} + \frac{q}{V}|\Delta\rho| \\ &= \frac{1}{t_d} + \frac{q\rho_0}{V}|\alpha_s S - \alpha_T T|,\end{aligned} \quad (25)$$

252 where  $V$  denotes the typical volume of the boxes.

253

The equations (23)–(24) are non-dimensionalised by scaling time with the diffusive time  $t_d$ , temperature with a characteristic temperature  $T^*$  and salinity with  $\alpha_T T^*/\alpha_S$ . Introducing  $\epsilon_a = t_r/t_d$  we arrive at

$$\dot{T} = -\frac{1}{\epsilon_a} (T - \Theta(t)) - T - \mu|S - T|T \quad (26)$$

$$\dot{S} = \sigma(t) - S - \mu|S - T|S. \quad (27)$$

254 Here  $\mu = t_d q \rho_0 T_0 \alpha_T / V$  and  $\sigma(t) = \alpha_S t_d (W_{\text{prec}}(t) + W_{\text{fresh}}(t)) / (\alpha_T T^* H)$ . We  
255 refer to (Cessi, 1994; Roebber, 1995) for typical parameters. Typical relaxation

times are  $t_r = 25$  days for the relaxation of the ocean surface,  $t_r = 5$  years for relaxation at a depth of 400 m,  $t_r = 10$  years for relaxation at a depth of 800 m and  $t_r = 75$  years for the relaxation of the deep ocean. If we use the relaxation time at a typical ocean depth of 400 m, we estimate  $t_r = 5$  years, which yields  $\epsilon_a = 0.0228$ . Depending on whether we choose the ocean surface, depths at 400 m, 800 m or the deep ocean we estimate  $\epsilon_a = \{3 \times 10^{-4}, 0.0228, 0.046, 0.34\}$ . The results presented in Section 5 are not sensitive to the choice of depth. The box model has a typical ocean depth of  $H = 4500$  m and the control volume is estimated as  $V = HL\delta_w$  where the typical meridional scale is  $L = 8,250$  km and the width of the western boundary current is roughly  $\delta_w = 300$  km. The typical density is  $\rho_0 = 1,029 \text{ kg m}^{-3}$ . The reference temperature is chosen to be  $T^* = 20^\circ\text{C}$ , and  $\alpha_T = 0.17 \times 10^{-3} \text{ C}^{-1}$  and  $\alpha_S = 0.75 \times 10^{-3} \text{ psu}^{-1}$ . The flux parameter  $\mu$  is the ratio between the advective time scale and the diffusive time scale with  $\mu = t_{ad}/t_d$ . The advective time scale is calculated as follows: The western boundary current transports  $B = 12 \text{ Sv} = 12 \times 10^6 \text{ m}^3 \text{ s}^{-1}$ . The advective time scale is then  $t_{ad} = HL\delta_w/B = 29.4$  years which yields  $\mu = 7.5$ . The freshwater flux in the North Atlantic is estimated as  $(W_{\text{prec}}(t) + W_{\text{fresh}})S_0 \approx 0.2 \text{ Sv}$  with  $S_0 = 35 \text{ psu}$  (Ganopolski and Rahmstorf, 2002). Hence  $\sigma = 0.95$ . The diffusive time-scale is estimated as  $t_d = L^2/\pi^2\kappa_H = 219$  years, where  $\kappa_H = 1000 \text{ m}^2 \text{ s}^{-1}$  is the horizontal diffusion coefficient. Since we scale with the diffusive time scale, one unit of time corresponds to 219 years, which defines the slow ocean time scale.

The Stommel box model exhibits bistability for certain parameter ranges with one stable solution being thermally controlled with  $q = T - S > 0$  and the other controlled by salinity with  $q < 0$ . Figure 4 shows the steady-state flow strength  $q = T - S$  as a function of the freshwater flux  $\sigma$ . We remark that for the parameters described above the Stommel box model (26)–(27) is very close to the saddle-node. In Section 5 we shall consider freshwater fluxes which allow for bistability with  $\sigma = 0.8$  and which support only a single stable solution with  $\sigma = 1.3$ .

## 4.2 Atmosphere model

We consider the Lorenz-84 model for the general circulation of the atmosphere (Lorenz, 1984, 1990)

$$\begin{aligned}\dot{x} &= -(y^2 + z^2) - a(x - F) \\ \dot{y} &= xy - bxz - (y - G) \\ \dot{z} &= bxy + xz - z,\end{aligned}\tag{28}$$

which evolves on the fastest time scale with typical times of the order of days. These equations describe the westerly zonal mean flow current with strength  $x$  and the amplitudes  $y, z$  of the cosine and sine waves of the mean circulation. The superimposed sine and cosine waves are advected by the mean flow, modelled here by the quadratic terms involving the factor  $b$ . The model describes how energy vacillates between a zonal jet stream and a meandering jet stream.  $F$  denotes the meridional temperature gradient and the model assumes that the zonal mean flow is in thermal balance, neglecting the effect of the eddies  $(y, z)$ . Similarly,  $G$  denotes the longitudinal temperature gradient, i.e. the heating gradient between land and

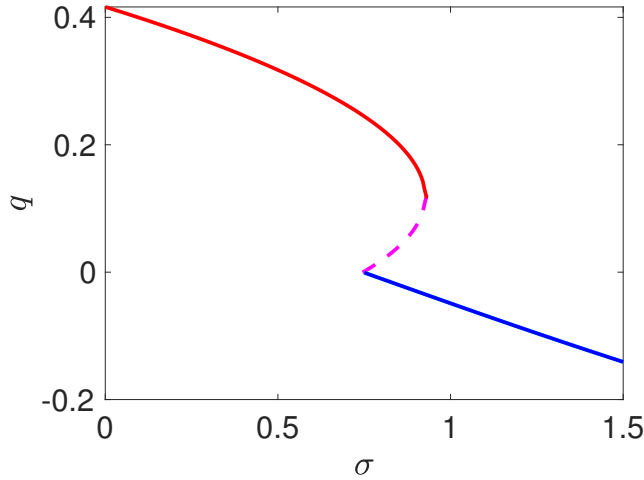


**Fig. 4** Flow strength  $q = T - S$  as a function of the freshwater flux  $\sigma$  for  $\mu = 7.5$ ,  $\Theta = 1$  and  $\epsilon_a = 0.34$  for the Stommel box model (26)–(27). The red branch depicts stable thermally driven steady states, the dashed curve depicts unstable solutions and the lower blue branch depicts salinity driven steady states. The Stommel box model exhibits bistability for  $\sigma \in [0.750, 0.94]$ .

295 sea, which is driving  $y$ . The model exhibits chaos depending on the parameters  
 296  $a$ ,  $b$ ,  $F$  and  $G$ . Reasonable time units in this model are 5 days and  $a < 1$  and  
 297  $b > 1$  (Lorenz, 1990). In Figure 3 the chaotic attractor is depicted for  $F = 8$ ,  
 298  $G = 1$ ,  $a = 0.25$  and  $b = 4$ . For each hemisphere we assume that the dynamics is  
 299 given by a Lorenz-84 system (28). The difference between the two hemispheres is  
 300 in how far the ocean and the sea-ice couple into the atmospheric model via the  
 301 meridional and zonal temperature gradients. In the Southern hemisphere the effect  
 302 of the Northern ocean and sea-ice is neglected and we assume constant temperature  
 303 gradients with  $F^{(S)} = F_0^{(S)}$  and  $G^{(S)} = G_0^{(S)}$ . In the Northern hemisphere, the  
 304 ocean and the atmosphere are coupled and we follow Roebber (1995) to couple the  
 305 Stommel box model (26)–(27) with the Lorenz-84 model (28). The coupling of the  
 306 fast atmosphere to the slow ocean occurs via the ambient atmospheric temperature  
 307 gradient  $\Theta$  and the freshwater influx  $\sigma$ . The backcoupling of the slow ocean to the  
 308 fast atmosphere occurs via the meridional and zonal temperature gradients  $F$  and  
 309  $G$ , respectively. We make the following assumptions (suppressing the superscript  
 310  $N$  denoting the Northern hemisphere):

- 311 (i) The meridional temperature gradient  $F$  in the Lorenz-84 model (28) is (in  
 312 the absence of sea-ice) approximated by the meridional temperature gradient  
 313 of the ocean  $T = T_e - T_p$  with  $F = F_0 + F_1 T$  with  $F_1 \geq 0$ .  
 314 (ii) The longitudinal gradient  $G$  in the Lorenz-84 model (28) is dominated by the  
 315 temperature difference of land and sea. Ignoring the diurnal cycle, we argue  
 316 that near the equator the land heats up more than the ocean whereas in the  
 317 polar region the ocean is warmer than the land (especially during winter).  
 318 Hence, an increased oceanic meridional temperature gradient  $T = T_e - T_p$   
 319 with warmer equatorial waters and colder polar waters, implies a decreased  
 320 longitudinal temperature gradient decreases. Hence the longitudinal temper-

- 321 ature gradient  $G$  in the Lorenz-84 model (28) is (in the absence of sea-ice)  
 322 modelled as  $G = G_0 - G_1 T$  with  $G_1 \geq 0$ .
- 323 (iii) The ambient temperature gradient  $\Theta(t) = \Theta_e(t) - \Theta_p(t)$  in the Stommel box  
 324 model (26)–(27) is given by thermal wind balance as  $\Theta = \theta x$  (in the absence  
 325 of sea-ice). Without sea-ice we would have  $\Theta = (x - F_0)/F_1$ .
- 326 (iv) The freshwater transport associated with evaporation and precipitation depends  
 327 on the strength of the atmospheric eddies and we set  $\sigma(t) = \sigma_0 +$   
 328  $\sigma_1(y^2 + z^2)$ . Here  $\sigma_0$  may be a function of time if freshwater fluxes stemming  
 329 from melting glaciers is included. In this work, however, we do not consider  
 330 any external freshwater flushes.

Introducing the eddy strength  $\Delta = y^2 + z^2$ , we summarise the ocean-atmosphere coupling as

$$\begin{aligned}
 F &= F_0 + F_1 T \\
 G &= G_0 - G_1 T \\
 \Theta(t) &= \theta_0 + \theta_1 \frac{x - \bar{x}}{\sqrt{\epsilon_f}} \\
 \sigma(t) &= \sigma_0 + \sigma_1 \frac{\Delta - \bar{\Delta}}{\sqrt{\epsilon_f}}.
 \end{aligned} \tag{29}$$

331 Here and in the following a bar denotes the average. The atmospheric driving  
 332 terms  $(x - \bar{x})/\sqrt{\epsilon_f}$  and  $(\Delta - \bar{\Delta})/\sqrt{\epsilon_f}$  converge to Brownian motion for  $\epsilon_f \rightarrow 0$  as  
 333 outlined in Section 3. They represent the stochastic forcing of the atmosphere on  
 334 the slow ocean dynamics.

### 335 4.3 Sea-ice model

336 The presence of sea-ice significantly changes the dynamics of the slower ocean and  
 337 the faster atmosphere. Sea-ice interacts with both the atmosphere and the ocean  
 338 in several ways. Sea-ice responds rapidly to changes in temperature and grows  
 339 on a typical time scale of a few months, placing its dynamics on an intermediate  
 340 time scale between the fast atmospheric dynamics and the slow ocean dynamics.  
 341 Sea-ice is created by colder polar ocean box temperatures  $T_p$ . Conversely, it is  
 342 melted by warmer polar ocean temperatures  $T_p$ . Furthermore, the meridional at-  
 343 mospheric heat flux plays a major role in the melting and preservation of sea-ice  
 344 (Monahan et al., 2008; Drijfhout et al., 2013; Kleppin et al., 2015). In particular,  
 345 meandering of the westerly Northern hemisphere jet stream enhances the merid-  
 346 ional atmospheric heat flux by warm eddies drawing warm tropical air into polar  
 347 regions. The degree of meandering of the jet stream is captured in our model by  
 348  $\Delta_N = y_N^2 + z_N^2$ . Banderas et al. (2012, 2015) showed that additionally Southern  
 349 Ocean winds, measured in our model by the strength of the zonal mean flow  $x_S$ ,  
 350 couple the southern and northern oceans via Ekman pumping thereby influencing  
 351 the sea-ice extent.

We parametrise the sea-ice cover by a variable  $\xi(t)$ . We consider here inter-  
 mittent sea-ice dynamics where the sea-ice cover exhibits sporadic brief periods of  
 extreme extent. To model such dynamics we employ a CAM process (6). Acknowl-  
 edging the atmospheric dynamics as a driver for the variations of sea-ice cover, we



propose the following deterministic approximation of a CAM process,

$$\epsilon_i \dot{\xi} = \left(\lambda + \frac{\kappa^2}{2}\right)\xi + \sqrt{\frac{\epsilon_i}{\epsilon_f}} \delta(\kappa\xi + g)(x_S - \bar{x}_S) + \sqrt{\frac{\epsilon_i}{\epsilon_f}} c(\Delta_N - \bar{\Delta}_N), \quad (30)$$

where the noise is deterministically generated by the chaotic atmospheric northern eddies  $\Delta_N(t)$  and the effect of the southern zonal jet stream  $x_S(t)$ . We assume for simplicity that this effect scales linearly with  $\Delta_N(t)$  and  $x_S(t)$ , respectively. According to the theory of deterministic homogenisation presented in Section 3, this ordinary differential equation converges for  $\epsilon_f \rightarrow 0$ , i.e. when the atmosphere is infinitely faster than the sea-ice dynamics, to the CAM stochastic differential equation

$$\epsilon_i d\xi = (\lambda + \kappa^2)\xi dt + (\kappa\xi + g) \circ dW_1 + \tilde{c} dW_2. \quad (31)$$

352 The limiting stochastic differential equation (31) corresponds to the CAM process  
 353 (6) with  $L = \lambda + \kappa^2/2$ ,  $E = \delta\eta_x\kappa$ ,  $B = \tilde{c} = \eta_\Delta c$  and  $G = \delta\eta_x g/(1 + E^2/(2L))$   
 354 and with  $y_\epsilon = \xi - A$  where  $A = EG/(2L)$ . Here  $\eta_{x,\Delta}$  are the standard devi-  
 355 ations of the noises  $W_x(t) = \lim_{\epsilon_f \rightarrow 0} \int^{t/\epsilon_f} (x_S(s) - \bar{x}_S) ds / \sqrt{\epsilon_f}$  and  $W_\Delta(t) =$   
 356  $\lim_{\epsilon_f \rightarrow 0} \int^{t/\epsilon_f} (\Delta_N(s) - \bar{\Delta}_N) ds / \sqrt{\epsilon_f}$ . Note that whereas actual sea-ice cover is a  
 357 bounded variable, the variable  $\xi(t)$  is unbounded. In this sense the CAM process  
 358 (30) (and its limiting dynamics (31)) does not model the actual extent of the  
 359 sea-ice but rather constitutes a conceptual model to account for the assumed in-  
 360 termittent nature of the sea-ice cover.

361

362 The influence of sea-ice on the ocean and atmosphere is manifold. Sea-ice acts  
 363 as a thermal insulator, preventing the exchange of heat from the ocean to the atmo-  
 364 sphere, thereby decreasing the meridional ocean temperature gradient  $T = T_e - T_p$ .  
 365 This effect plays a major role in our model and will be shown to be responsible for  
 366 the abrupt temperature changes. Once sea-ice has formed it prohibits precipitation  
 367 of evaporated water from the polar ocean on polar land mass, suppressing fresh-  
 368 water fluxes. Furthermore, during the formation of sea-ice salt is extruded into  
 369 the ocean during build up and freshwater is added into the ocean during melting.  
 370 Sea-ice affects both meridional and longitudinal temperature gradients of the at-  
 371 mosphere (i.e.  $F^{(N)}$  and  $G^{(N)}$  in our model). Increased sea-ice extent strengthens  
 372 the meridional thermal gradient experienced by the atmosphere, thereby increasing  
 373 the zonal mean-flow component  $x_N$ . Similarly, an increased sea-ice extent leads to  
 374 a decreased longitudinal thermal gradient experienced by the atmosphere, thereby  
 375 decreasing  $G$  (again favouring zonal flow  $x_N$ ). This motivates to augment the  
 376 expressions for the meridional and longitudinal temperature gradients of the at-  
 377 mosphere  $F$  and  $G$  in the Lorenz-84 model (28) (for the Northern hemisphere)  
 378 and the ambient oceanic temperature gradient  $\Theta$  and the freshwater flux  $\sigma$  in the  
 379 Stommel box model (26)–(27). In particular we note (suppressing the superscript  
 380  $N$ ):

- (i) The meridional thermal gradient in the Northern hemisphere is given by the ocean temperature gradient  $T$  if there is no sea-ice ( $\xi = 0$ ) and is increased by sea-ice  $\xi > 0$  independent of the ocean temperature gradient:

$$F = F_0 + F_1 T + F_2 \xi, \quad (32)$$

381 with  $F_{1,2} \geq 0$ . Note that in the case of sea-ice  $\xi > 0$ , the equatorial sea tem-  
 382 perature  $T_e$  continues to contribute to the thermal gradient, so the oceanic  
 383 temperature gradient  $T$  is still affecting  $F$  with  $F_1 \neq 0$  even in the presence  
 384 of sea-ice.

- (ii) The longitudinal thermal gradient in the Northern hemisphere is dominated  
 by the ocean temperature gradient  $T$  if there is no sea-ice ( $\xi = 0$ ) and is  
 decreased by sea-ice  $\xi > 0$  independent of the ocean temperature gradient

$$G = G_0 - G_1 T - G_2 \xi, \quad (33)$$

385 with  $G_{1,2} \geq 0$ . As for the meridional thermal gradient discussed above in (i),  
 386 the land-sea temperature gradient at the equator is still determined by the  
 387 equatorial ocean temperature  $T_e$ , so the oceanic temperature gradient  $T$  is  
 388 still affecting  $G$  with  $G_1 \neq 0$  even in the presence of sea-ice.

- (iii) The atmospheric temperature gradient  $\Theta(t) = \theta x$  is maintained by thermal  
 389 balance, so only indirectly affected by sea-ice. To account for the insulating  
 390 effect of sea-ice a damping term proportional to  $(\xi - \bar{\xi})T$ , where  $\bar{\xi}$  denotes  
 391 the mean of the sea-ice cover variable  $\xi$ , is added to the temperature gradient  
 392 equation (26). This term (cf. (13)) is the key dynamical ingredient for the  
 393 generation of abrupt sharp temperature changes in our model, resembling DO  
 394 events. To highlight the role of the intermittent sea-ice events we introduce  
 395 a thresholded driver  $\Xi(\xi) = \max(\xi, \xi^*)$  which filters out small fluctuations  
 396 with  $\xi < \xi^*$ . We shall use this thresholded driver, upon subtracting its mean  
 397  $\bar{\Xi}$ , to enter the ocean dynamics and consider a damping term of the form  
 398  $(\Xi(t) - \bar{\Xi})T$  in the temperature gradient equation (26).  
 399

- (iv) The source term of salinity decreases during growth of sea-ice and increases  
 during melting of sea-ice. We set

$$\sigma(t) = \sigma_0 + \sigma_1(y^2 + z^2) - \sigma_2 \dot{\xi}. \quad (34)$$

400 Summarising we motivated the proposed coupled ocean-atmosphere and sea-ice  
 401 model (13)–(18) with the interactions captured in (19)–(22), which are expressed  
 402 by (32)–(34). In the next section we will illustrate how this model is able to  
 403 reproduce abrupt temperature changes as in DO events.

## 404 5 Illustration of the model

405 We now show numerical simulations of the conceptual coupled ocean-atmosphere  
 406 and sea-ice model (13)–(18). We focus here on the effect of intermittent sea-ice on  
 407 the oceanic temperature gradient  $T$  through insulation, as expressed by the linear  
 408 damping term in (13).

409 In the Stommel box model we set  $\mu = 7.5$  and set  $\epsilon_a = 0.34$ , corresponding  
 410 to the relaxation time in the deep ocean (we have checked that our results do not  
 411 depend qualitatively when varying  $\epsilon_a$ ). We choose as base ambient temperature  
 412 gradient  $\theta_0 = 1$  and as base freshwater flux we consider here  $\sigma_0 = 0.8$  for which  
 413 the uncoupled Stommel box model exhibits bistability and  $\sigma_0 = 1.3$  for which only  
 414 a single stable solution exists (cf. Figure 4). The perturbations to these base states  
 415 induced by atmospheric noise are set to  $\theta_1 = 0.01/\eta_x$  and  $\sigma_1 = 0.01/\eta_\Delta$  and ne-  
 416 glect the effect of sea-ice on the freshwater flux setting  $\sigma_2 = 0$ . We further suppress

417 the backcoupling of the slow ocean dynamics onto the fast atmospheric dynamics  
 418 by setting  $F_1 = G_1 = 0$ . The standard deviations of the atmospheric noise associ-  
 419 ated with zonal mean flow  $x$  and the large-scale eddies  $\Delta$ , respectively,  $\eta_x = 0.513$   
 420 and  $\eta_\Delta = 0.071$ , were estimated from a long time-integration of the Lorenz-84  
 421 model. The atmosphere is kept in perpetual winter conditions with  $F_0 = 8$  and  
 422  $G_0 = 1$  and with  $a = 0.25$  and  $b = 4$  (Lorenz, 1984). We choose for simplicity  
 423 the same values of the parameters  $a, b, F_0, G_0$  for the Northern and the Southern  
 424 hemisphere. This is not necessary; the only requirement in the derivation of the  
 425 deterministic approximation of the CAM noise model for sea-ice is that the north-  
 426 ern and southern atmospheric dynamics are sufficiently decorrelated which can be  
 427 achieved using the same equation parameters but different initial conditions. The  
 428 sea-ice is coupled to the Stommel two-box model with  $d = 50$ , and its parameters  
 429 are set to  $\kappa = 1.118$ ,  $\lambda = -1.565$ ,  $g = 0.3351$ ,  $\delta = 1/\sigma_1$  and  $c = 0.3/\eta_2$ . Similarly  
 430 the mean values  $\bar{x} = 1.0147$ ,  $\bar{\Delta} = 1.7463$  and  $\bar{\xi} = 0.12$  were estimated from long  
 431 time simulations of the Lorenz-84 model and the sea-ice model. Note that in the  
 432 limit  $\epsilon_f \rightarrow 0$  we expect  $\bar{\xi} = 0$ . The physical set-up suggests that in the Stommel  
 433 box model a unit of time corresponds to 219 years, and that the time-scale par-  
 434 ameters controlling the time-scales of the fastest atmospheric processes and the  
 435 intermediate time scale of the sea-ice are  $\epsilon_f = 0.0083$  and  $\epsilon_i = 0.05$  (cf. (10)).  
 436

We first illustrate the various statistical limit laws which give rise to the ef-  
 fective stochastic behaviour of the deterministic coupled ocean-atmosphere and  
 sea-ice model (13)–(18). We confirm the deterministic approximation of stochastic  
 Gaussian processes  $W_t$  by

$$W_x(t) = \frac{1}{\sqrt{\epsilon_f}} \int_0^{\frac{t}{\epsilon_f}} (x(s) - \bar{x}) ds \quad (35)$$

$$W_\Delta(t) = \frac{1}{\sqrt{\epsilon_f}} \int_0^{\frac{t}{\epsilon_f}} (\Delta(s) - \bar{\Delta}) ds, \quad (36)$$

and of the Lévy processes  $L_{\alpha,\eta,\beta}$  by

$$L_\xi(t) = \frac{1}{\epsilon_i^{1-\gamma}} \int_0^{\frac{t}{\epsilon_i}} (\xi(s) - \bar{\xi}) ds, \quad (37)$$

437 with  $\gamma = 1/\alpha$ . These constitute the noise processes driving the coupled model  
 438 (13)–(18). We show results in Figure 5 for the approximation of Gaussian noise  
 439  $W_\Delta$  (plots for  $W_x$  look similar). Figure 6 shows a realisation of the time series  
 440 of the sea-ice variable  $\xi(t)$  obtained from (15), as well as the thresholded driver  
 441  $\Xi(\xi)$  which captures the intermittent large sea-ice cover events above the thresh-  
 442 old  $\xi^* = 6$ . The corresponding integrated noise approximation  $L_\Xi$  is shown in  
 443 Figure 7. The parameters chosen for the sea-ice model (15) imply  $\alpha = 1.5$  and  
 444  $\beta = 0.99$  (cf. (7) and (8)). The integrated CAM-process  $L_\xi$  and the thresholded  
 445 version  $L_\Xi$  exhibit almost exclusively positive jumps as predicted by the homogeni-  
 446 sation theory results which yields  $\beta = 0.99$ .  
 447

448 The effect of these jumps on the ocean's temperature gradient  $T$  is illustrated  
 449 in Figure 8 where we show results for  $\sigma_0 = 0.8$  and for  $\sigma_0 = 1.3$ . For  $\sigma_0 = 0.8$   
 450 the uncoupled Stommel box model supports two stable solutions, and the abrupt

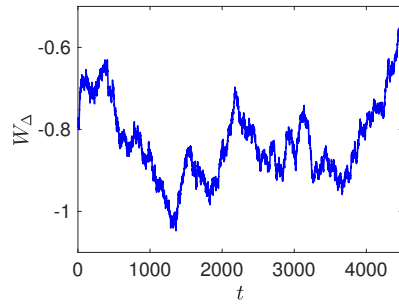


**Fig. 5** Time series of  $W_{\Delta}$  (36) approximating Gaussian noise.

451 changes are shown as deviations of the interstadial solution which is characterised  
 452 by a positive thermally-driven flux  $q = T - S > 0$ . For  $\sigma_0 = 1.3$  the Stommel box  
 453 model only supports a single solution which is characterised by negative salinity-  
 454 driven flux  $q < 0$ . In both cases, the  $\alpha$ -stable driver  $L_{\Xi}$  leads to significant sharp  
 455 drops on the meridional temperature gradient  $T = T_e - T_p$ , implying sharp in-  
 456 creases of the oceanic polar temperature  $T_p$ . At  $t \approx 14,300$  this is particularly  
 457 strong with a change in temperature of more than  $7^{\circ}\text{C}$  (the Stommel model is  
 458 normalised such that  $T = 1$  corresponds to  $20^{\circ}\text{C}$ ). This large and abrupt change is  
 459 caused by the large jump of  $L_{\xi}$  which itself is caused by a prolonged period of large  
 460 sea-ice cover events  $\xi$  (cf. Figure 7). These temperature increases gradually decay  
 461 to the (noisy) steady interstadial state. The time between events is here roughly  
 462 1,800 years, which is the same order of magnitude as observed in ice-core records.  
 463 The corresponding time-series for the salinity  $S(t)$  and the flux  $q(t) = T - S$   
 464 are shown in Figure 9 and Figure 10. Whereas the salinity gradient increases for  
 465  $\sigma_0 = 0.8$  it decreases for  $\sigma_0 = 1.3$  during the abrupt changes. In both cases, the  
 466 resulting flux  $q$  decreases, implying a more salinity-driven transport during the  
 467 abrupt changes.

468

469 An application of the  $p$ -variation test, described in Section 2, determines the  
 470 stability parameter of the time-series for the meridional temperature gradient  $T$   
 471 as  $\alpha = 1.8$  for  $\sigma_0 = 0.8$  and  $\alpha = 1.75$  for  $\sigma_0 = 1.3$ , consistent with the value  
 472 of  $\alpha = 1.78$  obtained in Section 2 from  $\text{Ca}^{2+}$  ice-core data and the results by  
 473 Ditlevsen (1999). The small fluctuations of  $T$  and  $S$  are induced by fast atmo-  
 474 spheric (Brownian) noise with  $\theta_1 \neq 0$  and  $\sigma - 1 \neq 0$ , respectively.

475

## 476 6 Discussion

477 We developed a self-consistent conceptual model of a slow ocean coupled to a fast  
 478 atmosphere and to sea-ice, which evolves on an intermediate time scale and is  
 479 driven by the atmosphere. The model relates the abrupt climate changes of DO  
 480 events to intermittent sea-ice dynamics and the sporadic occurrence of large sea-  
 481 ice extent. The intermittency in the sea-ice model is induced by synergetic forcing  
 482 by fast atmospheric Northern hemisphere eddy activity and by fast atmospheric

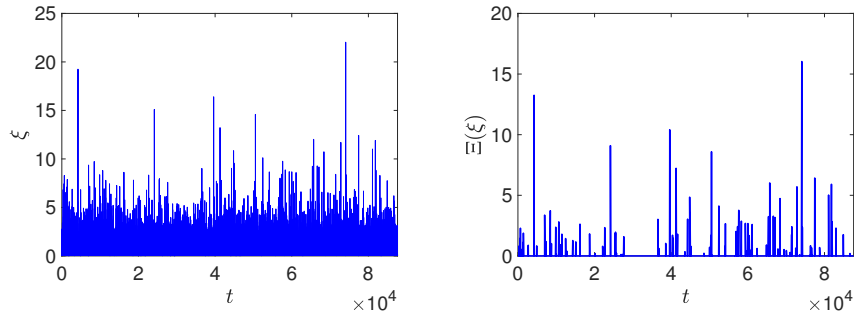


**Fig. 6** Left: Time series of the sea-ice variable  $\xi(t)$  approximating CAM noise. Right: Time series of the associated threshold time series  $\Xi(\xi) = \max(\xi, 6) - 6$ .

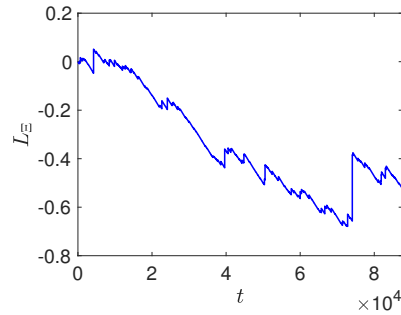


**Fig. 7** Integrated noise  $L_{\Xi}$  (37) approximating and  $\alpha$ -stable process with  $\alpha = 1.5$  and  $\beta = 0.99$  for the time series  $\Xi(\xi)$  depicted in Figure 6.

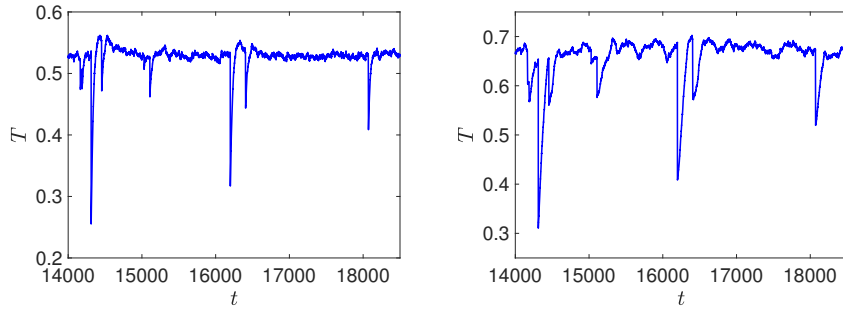


**Fig. 8** Time-series of the oceanic meridional temperature gradient  $T$  obtained by integration of the model (13) driven by the sea-ice time-series depicted in Figure 6. Left:  $\sigma_0 = 0.8$ . Right:  $\sigma_0 = 1.3$ .

483 Southern hemisphere zonal mean flow. The sea-ice then acts on the slow ocean by  
 484 insulating it, preventing the heat exchange of the polar ocean with the atmosphere.  
 485 Using statistical limit laws for deterministic chaotic dynamical systems the sea-ice  
 486 model was shown to generate non-Gaussian  $\alpha$ -stable noise, consistent with the time  
 487 series analysis of ice core data (Ditlevsen, 1999). The apparent regularity of the  
 488 temporal spacing between successive Dansgaard-Oeschger events deduced from

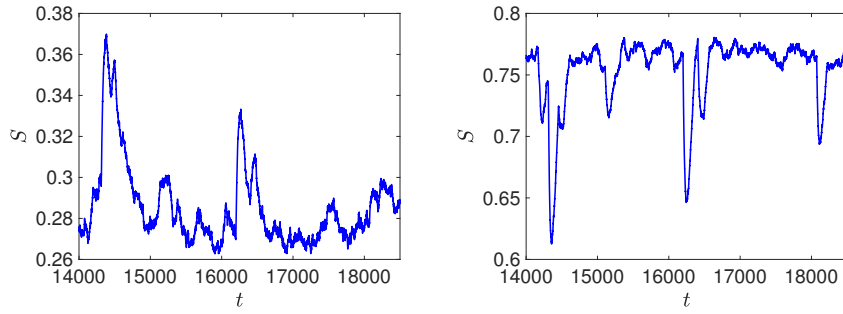


**Fig. 9** Time-series of the salinity  $S$  obtained by integration of the model (13) driven by the sea-ice time-series depicted in Figure 6. Left:  $\sigma_0 = 0.8$ . Right:  $\sigma_0 = 1.3$ .

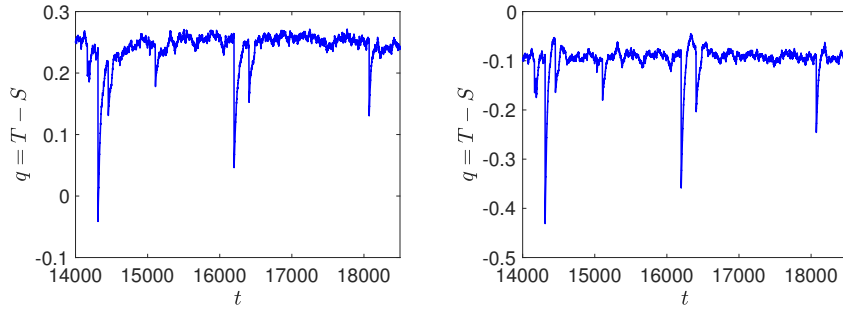


**Fig. 10** Time-series of the flux  $q = T - S$  obtained by integration of the model (13) driven by the sea-ice time-series depicted in Figure 6. Left:  $\sigma_0 = 0.8$ . Right:  $\sigma_0 = 1.3$ .

489 the ice-core data (Grootes and Stuiver, 1997; Yiou et al., 1997; Ditlevsen et al.,  
 490 2005), is here not caused by any inherent periodicity in the system but rather  
 491 by the random occurrence of extreme sea-ice extents above a certain threshold  
 492 below which the response of the ocean is not significant. This is in accordance  
 493 with Ditlevsen et al. (2007) who showed that there is no statistically significant  
 494 evidence for strict periodicity.

495

496 The particular signature of the temperature with its abrupt warming events is  
 497 caused by an intermittent process evolving on a faster time scale than the oceanic  
 498 time scale. In our model here this process is provided by (the approximation of)  
 499 a CAM process  $\xi$  (cf (30)) which quantifies the variability in the sea-ice cover.  
 500 The integrated CAM noise in the variable the gives rise to non-Gaussian  $\alpha$ -stable  
 501 statistics with the jumps corresponding to the abrupt warming events. The CAM  
 502 noise itself was dynamically induced by fast atmospheric noise. It is pertinent to  
 503 mention that one could equally consider other intermittent mechanisms than sea-  
 504 ice cover variability such as intermittent freshwater influxes. In this case the CAM  
 505 noise would enter the salinity equation (13) via the freshwater source terms in  $\sigma(t)$   
 506 (22), and the CAM noise would be a conceptual model for intermittent freshwater  
 507 changes, captured by  $\hat{\xi}$ .

508

509 The model hinges on statistical limit laws. These laws were invoked to gener-  
510 ate both the Brownian noise as well as the non-Gaussian  $\alpha$ -stable noise. Statistical  
511 limit laws describe the statistical properties of integrals (or sums) of observables.  
512 The observables here are observables of (relatively) fast variables. The integrals  
513 over the observables naturally arise in the multi-scale context when the faster  
514 variables are integrated in the slower dynamics. The simplest statistical limit law  
515 is the law of large numbers, which ensures that appropriately scaled variables  
516 (here our observables) converge to a deterministic limit, their average. The cen-  
517 tral limit theorem and its generalisations allows precise statements on fluctuations  
518 around the mean behaviour. Whereas statistical limit laws are part of the stan-  
519 dard tool box when the observations are of a stochastic nature, and in particular  
520 when the observations are independent identically distributed random variables.  
521 The case of integrals (or sums) of deterministic chaotic observables has only been  
522 recently explored. These studies provide a rigorous justification why scientists can  
523 parametrise the effect of unresolved scales, such as the effect of fast weather on  
524 the slow ocean, by noise as proclaimed by Hasselmann (1976) and Leith (1975) in  
525 the context of climate dynamics. Rather than just providing a general qualitative  
526 framework, statistical limit theorems and homogenisation theory provide precise  
527 statements on the nature of the noise – i.e. is the noise Brownian or  $\alpha$ -stable, is  
528 it additive or multiplicative, and is the noise to be interpreted in the sense of Itô  
529 or of Stratonovich/Marcus? Furthermore, homogenisation theory provides explicit  
530 expressions for the drift and diffusion coefficients of the limiting stochastic dif-  
531 ferential equation. Recently, at least formally, statistical limit laws were extended  
532 to the more realistic case of finite time-scale separation (Wouters and Gottwald,  
533 2019a,b). The typical application of statistical limit laws in the geosciences is to  
534 provide closed equations for resolved variables of interest by parametrising unre-  
535 solved fast and/or small-scale degrees of freedom by noise. The reward for such a  
536 parametrisation is of a computational nature as one now only needs to simulate  
537 an equation on the slow time scale, avoiding prohibitively small time steps needed  
538 to control numerical instabilities of the fast dynamics.

539 Here we pursue a conceptionally different route. Rather than starting from a  
540 deterministic dynamical system to derive a limiting stochastic dynamical system,  
541 we reverse the order and use statistical limit laws to determine dynamical mecha-  
542 nisms which are consistent with the statistical properties of the observations. We  
543 use statistical limit laws in the sense of reverse engineering, thereby identifying  
544 key dynamical mechanisms for DO events such as intermittency, provided by sea-  
545 ice variability on an intermediate time-scale. Statistical limit laws allowed us to  
546 both generate the intermittent process in the first place (here we used atmospheric  
547 noise to generate the intermittent CAM process for the sea-ice dynamics) as well as  
548 generating the  $\alpha$ -stable process driving the slow ocean dynamics with its abrupt  
549 climate changes. The former was achieved by central limit theorems generating  
550 Brownian motion, the latter by a generalised central limit theorem generating  
551 non-Gaussian Lévy processes.

552 **Acknowledgements** The ice core data were generously provided by Peter Ditlevsen. I am  
553 grateful to Armin Köhl, Johannes Lohmann, Marisa Montoya and Xu Zhang for many inter-  
554 esting and helpful discussions. I would like to thank Cameron Duncan, Nathan Duingan and  
555 Eric Huang who explored the  $p$ -variation test and suitable parameter ranges of the Lorenz-84

556 system in a summer project in 2014 at an early stage of this work. I would like to thank Peter  
557 Ditlevsen and an anonymous referee for their valuable comments.

## 558 References

- 559 Andersen KK, Azuma N, Barnola JM, Bigler M, Biscaye P, Caillon N, Chappel-  
560 laz J, Clausen HB, Dahl-Jensen D, Fischer H, Flückiger J, Fritzsche D, Fujii  
561 Y, Goto-Azuma K, Grønvold K, Gundestrup NS, Hansson M, Huber C, Hvid-  
562 berg CS, Johnsen SJ, Jonsell U, Jouzel J, Kipfstuhl S, Landais A, Leuenberger  
563 M, Lorrain R, Masson-Delmotte V, Miller H, Motoyama H, Narita H, Popp T,  
564 Rasmussen SO, Raynaud D, Rothlisberger R, Ruth U, Samyn D, Schwander J,  
565 Shoji H, Siggaard-Andersen ML, Steffensen JP, Stocker T, Sveinbjörnsdóttir AE,  
566 Svensson A, Takata M, Tison JL, Thorsteinsson T, Watanabe O, Wilhelms F,  
567 White JWC, members NGICP (2004) High-resolution record of Northern Hemi-  
568 sphere climate extending into the last interglacial period. *Nature* 431(7005):147–  
569 151
- 570 Andersen KK, Svensson A, Johnsen SJ, Rasmussen SO, Bigler M, Röthlisberger  
571 R, Ruth U, Siggaard-Andersen ML, Steffensen JP, Dahl-Jensen D, Vinther BM,  
572 Clausen HB (2006) The Greenland ice core chronology 2005, 15–42 ka. Part 1:  
573 constructing the time scale. *Quaternary Science Reviews* 25(23):3246 – 3257,  
574 critical Quaternary Stratigraphy
- 575 Applebaum D (2009) Lévy processes and stochastic calculus, Cambridge Stud-  
576 ies in Advanced Mathematics, vol 116, 2nd edn. Cambridge University Press,  
577 Cambridge
- 578 Banderas R, Álvarez-Solas J, Montoya M (2012) Role of CO<sub>2</sub> and Southern Ocean  
579 winds in glacial abrupt climate change. *Climate of the Past* 8(3):1011–1021
- 580 Banderas R, Alvarez-Solas J, Robinson A, Montoya M (2015) An interhemispheric  
581 mechanism for glacial abrupt climate change. *Climate Dynamics* 44(9):2897–  
582 2908
- 583 Boers N, Ghil M, Rousseau DD (2018) Ocean circulation, ice shelf, and sea ice  
584 interactions explain Dansgaard–Oeschger cycles. *Proceedings of the National*  
585 *Academy of Sciences* 115(47):E11005–E11014
- 586 Cessi P (1994) A simple box model of stochastically forced thermohaline flow.  
587 *Journal of Physical Oceanography* 24(9):1911–1920
- 588 Chechkin A, Pavlyukevich I (2014) Marcus versus Stratonovich for systems with  
589 jump noise. *Journal of Physics A: Mathematical and Theoretical* 47(34):342001
- 590 Chechkin AV, Metzler R, Klafter J, Gonchar VY (2008) Introduction to the theory  
591 of Lévy flights. In: Klages R, Radons G, Sokolov IM (eds) *Anomalous Transport*,  
592 Wiley-VCH Verlag GmbH & Co. KGaA, pp 129–162
- 593 Chevyrev I, Friz PK, Korepanov A, Melbourne I (2019) Superdiffusive limits for  
594 deterministic fast-slow dynamical systems. arXiv 1907.04825, 1907.04825
- 595 Crucifix M (2012) Oscillators and relaxation phenomena in Pleistocene climate  
596 theory. *Philosophical Transactions of the Royal Society of London A: Mathe-*  
597 *matical, Physical and Engineering Sciences* 370(1962):1140–1165
- 598 Dansgaard W, Johnsen S, Clausen HB, Dahl-Jensen D, Gundestrup N, Hammer H,  
599 Oeschger H (1984) North Atlantic climate oscillations revealed by deep Greenland  
600 ice cores. *Climate Processes and Climate Sensitivity, Geophys Monogr* 5:288–  
601 298



- 602 Deser C, Holland M, Reverdin G, Timlin M (2002) Decadal variations in Labrador  
603 sea ice cover and North Atlantic sea surface temperatures. *Journal of Geophys-*  
604 *ical Research: Oceans* 107(C5):3–1–3–12
- 605 Ditlevsen PD (1999) Observation of  $\alpha$ -stable noise induced millennial climate  
606 changes from an ice-core record. *Geophysical Research Letters* 26(10):1441–1444
- 607 Ditlevsen PD, Kristensen MS, Andersen KK (2005) The Recurrence Time of  
608 Dansgaard–Oeschger Events and Limits on the Possible Periodic Component.  
609 *Journal of Climate* 18(14):2594–2603
- 610 Ditlevsen PD, Andersen KK, Svensson A (2007) The DO-climate events are prob-  
611 ably noise induced: statistical investigation of the claimed 1470 years cycle.  
612 *Climate of the Past* 3(1):129–134
- 613 Dokken TM, Nisancioglu KH, Li C, Battisti DS, Kissel C (2013) Dansgaard-  
614 Oeschger cycles: Interactions between ocean and sea ice intrinsic to the Nordic  
615 seas. *Paleoceanography* 28(3):491–502
- 616 Drijfhout S, Gleeson E, Dijkstra HA, Livina V (2013) Spontaneous abrupt climate  
617 change due to an atmospheric blocking–sea-ice–ocean feedback in an unforced  
618 climate model simulation. *Proceedings of the National Academy of Sciences*  
619 110(49):19713–19718
- 620 Fang Z, Wallace JM (1994) Arctic sea ice variability on a timescale of weeks and  
621 its relation to atmospheric forcing. *Journal of Climate* 7(12):1897–1914
- 622 Friedrich T, Timmermann A, Menviel L, Elison Timm O, Mouchet A, Roche  
623 DM (2010) The mechanism behind internally generated centennial-to-millennial  
624 scale climate variability in an earth system model of intermediate complexity.  
625 *Geoscientific Model Development* 3(2):377–389
- 626 Fuhrer K, Neftel A, Anklin M, Maggi V (1993) Continuous measurements of hydro-  
627 gen peroxide, formaldehyde, calcium and ammonium concentrations along the  
628 new GRIP ice core from Summit, Central Greenland. *Atmospheric Environment*  
629 27A:1873–1880
- 630 Ganopolski A, Rahmstorf S (2001) Rapid changes of glacial climate simulated in  
631 a coupled climate model. *Nature* 409(6817):153–158
- 632 Ganopolski A, Rahmstorf S (2002) Abrupt glacial climate changes due to stochas-  
633 tic resonance. *Physical Review Letters* 88(3):153–158
- 634 Gardiner CW (2003) *Handbook of Stochastic Methods for Physics, Chemistry, and*  
635 *the Natural Sciences*, 3rd edn. Springer, New York
- 636 Gaspard P, Wang XJ (1988) Sporadicity: Between periodic and chaotic dynamical  
637 behaviours. *Proceedings of the National Academy of Sciences* 85:4591–4595
- 638 Gildor H, Tziperman E (2003) Sea-ice switches and abrupt climate change. *Philo-*  
639 *sophical Transactions of the Royal Society of London Series A: Mathematical,*  
640 *Physical and Engineering Sciences* 361(1810):1935–1944
- 641 Givon D, Kupferman R, Stuart A (2004) Extracting macroscopic dynamics: Model  
642 problems and algorithms. *Nonlinearity* 17(6):R55–127
- 643 Gottwald G, Crommelin D, Franzke C (2017) Stochastic climate theory. In:  
644 Franzke CLE, O’Kane TJ (eds) *Nonlinear and Stochastic Climate Dynamics*,  
645 Cambridge University Press, Cambridge, pp 209–240
- 646 Gottwald GA, Melbourne I (2013a) A Huygens principle for diffusion and anom-  
647 alous diffusion in spatially extended systems. *Proc Natl Acad Sci USA* 110:8411–  
648 8416
- 649 Gottwald GA, Melbourne I (2013b) Homogenization for deterministic maps and  
650 multiplicative noise. *Proceedings of the Royal Society A: Mathematical, Physical*

- 651 and Engineering Science 469(2156)
- 652 Gottwald GA, Melbourne I (2016) On the detection of superdiffusive behaviour  
653 in time series. *Journal of Statistical Mechanics: Theory and Experiment*  
654 2016(12):123205
- 655 Gottwald GA, Melbourne I (2020) Simulation of non-Lipschitz stochastic differ-  
656 ential equations driven by  $\alpha$ -stable noise: a method based on deterministic ho-  
657 mogenisation. arXiv 2004.09914
- 658 Gouëzel S (2004) Central limit theorem and stable laws for intermittent maps.  
659 *Probability Theory and Related Fields* 128:82–122
- 660 Greenland Ice-core Project (GRIP) Members (1993) Climate instability during the  
661 last interglacial period recorded in the GRIP ice core. *Nature* 364(6434):203–207
- 662 Grootes PM, Stuiver M (1997) Oxygen 18/16 variability in Greenland snow and ice  
663 with  $10^{-3}$  to  $10^5$ -year time resolution. *Journal of Geophysical Research: Oceans*  
664 102(C12):26455–26470
- 665 Haarsma RJ, Opsteegh JD, Selten FM, Wang X (2001) Rapid transitions and  
666 ultra-low frequency behaviour in a 40-kyr integration with a coupled climate  
667 model of intermediate complexity. *Climate Dynamics* 17(7):559–570
- 668 Hasselmann K (1976) Stochastic climate models. Part 1: Theory. *Tellus* 28(6):473–  
669 485
- 670 Hein C, Imkeller P, Pavlyukevich I (2009) Limit theorems for  $p$ -variations of so-  
671 lutions of SDEs driven by additive stable Lévy noise and model selection for  
672 paleo-climatic data. In: Duan J, Luo S, Wang C (eds) *Recent Development in*  
673 *Stochastic Dynamics and Stochastic Analysis, Interdisciplinary Math. Sciences,*  
674 *vol 8*, World Scientific, Singapore, pp 137–150
- 675 Hoff U, Rasmussen TL, Stein R, Ezat MM, Fahl K (2016) Sea ice and millennial-  
676 scale climate variability in the Nordic seas 90 kyr ago to present. *Nature Com-*  
677 *munications* 7(1):12247
- 678 Jensen MF, Nilsson J, Nisancioglu KH (2016) The interaction between sea ice  
679 and salinity-dominated ocean circulation: implications for halocline stability and  
680 rapid changes of sea ice cover. *Climate Dynamics* 47(9):3301–3317
- 681 Kelly D, Melbourne I (2016) Smooth approximation of stochastic differential equa-  
682 tions. *Ann Probab* 44(1):479–520
- 683 Kelly D, Melbourne I (2017) Deterministic homogenization for fast-slow systems  
684 with chaotic noise. *J Funct Anal* 272(10):4063–4102
- 685 Kleppin H, Jochum M, Otto-Bliesner B, Shields CA, Yeager S (2015) Stochas-  
686 tic atmospheric forcing as a cause of Greenland climate transitions. *Journal of*  
687 *Climate* 28(19):7741–7763
- 688 Kuske R, Keller JB (2001) Rate of convergence to a stable law. *SIAM Journal on*  
689 *Applied Mathematics* 61(4):1308–1323
- 690 Kwasniok F, Lohmann G (2009) Deriving dynamical models from paleoclimatic  
691 records: Application to glacial millennial-scale climate variability. *Physical Re-*  
692 *view E* 80(6):066104
- 693 Leith CE (1975) Climate response and fluctuation dissipation. *Journal of the At-*  
694 *mospheric Sciences* 32(10):2022–2026
- 695 Li C, Born A (2019) Coupled atmosphere-ice-ocean dynamics in Dansgaard-  
696 Oeschger events. *Quaternary Science Reviews* 203:1–20
- 697 Li C, Battisti DS, Schrag DP, Tziperman E (2005) Abrupt climate shifts in Green-  
698 land due to displacements of the sea ice edge. *Geophysical Research Letters*  
699 32(19)

- 700 Lohmann J, Ditlevsen PD (2019) A consistent statistical model selection for abrupt  
701 glacial climate changes. *Climate Dynamics* 52(11):6411–6426
- 702 Lorenz EN (1984) Irregularity: a fundamental property of the atmosphere. *Tellus*  
703 *A* 36A(2):98–110
- 704 Lorenz EN (1990) Can chaos and intransitivity lead to interannual variability?  
705 *Tellus A* 42(3):378–389
- 706 Magdziarz M, Klafter J (2010) Detecting origins of subdiffusion:  $p$ -variation test  
707 for confined systems. *Phys Rev E* 82:011129
- 708 Magdziarz M, Weron A, Burnecki K, Klafter J (2009) Fractional Brownian motion  
709 versus the continuous-time random walk: A simple test for subdiffusive  
710 dynamics. *Phys Rev Lett* 103:180602
- 711 Majda AJ, Franzke C, Crommelin D (2009) Normal forms for reduced stochastic  
712 climate models. *Proceedings of the National Academy of Sciences* 106(10):3649–  
713 3653
- 714 Manabe S, Stouffer R (2011) Are two modes of thermohaline circulation stable?  
715 *Tellus A* 51(3):400–411
- 716 Marcus S (1981) Modeling and approximation of stochastic differential equations  
717 driven by semimartingales. *Stochastics* 4:223–245
- 718 Meissner KJ, Eby M, Weaver AJ, Saenko OA (2008) CO<sub>2</sub> threshold for millennial-  
719 scale oscillations in the climate system: implications for global warming scenar-  
720 ios. *Climate Dynamics* 30(2-3):161–174
- 721 Melbourne I, Nicol M (2005) Almost sure invariance principle for nonuniformly  
722 hyperbolic systems. *Commun Math Phys* 260:131–146
- 723 Melbourne I, Nicol M (2009) A vector-valued almost sure invariance principle for  
724 hyperbolic dynamical systems. *Annals of Probability* 37:478–505
- 725 Melbourne I, Stuart A (2011) A note on diffusion limits of chaotic skew-product  
726 flows. *Nonlinearity* 24:1361–1367
- 727 Monahan AH, Alexander J, Weaver AJ (2008) Stochastic models of the meridional  
728 overturning circulation: time scales and patterns of variability. *Philosophical*  
729 *Transactions of the Royal Society of London A: Mathematical, Physical and*  
730 *Engineering Sciences* 366(1875):2525–2542
- 731 Penland C, Sardeshmukh PD (2012) Alternative interpretations of power-law dis-  
732 tributions found in nature. *Chaos: An Interdisciplinary Journal of Nonlinear*  
733 *Science* 22(2):023119
- 734 Petersen SV, Schrag DP, Clark PU (2013) A new mechanism for Dansgaard-  
735 Oeschger cycles. *Paleoceanography* 28(1):24–30
- 736 Rasmussen SO, Andersen KK, Svensson AM, Steffensen JP, Vinther BM, Clausen  
737 HB, Siggaard-Andersen ML, Johnsen SJ, Larsen LB, Dahl-Jensen D, Bigler M,  
738 Röthlisberger R, Fischer H, Goto-Azuma K, Hansson ME, Ruth U (2006) A  
739 new Greenland ice core chronology for the last glacial termination. *Journal of*  
740 *Geophysical Research: Atmospheres* 111(D6)
- 741 Roebber PJ (1995) Climate variability in a low-order coupled atmosphere-ocean  
742 model. *Tellus A* 47(4):473–494
- 743 Sadatzki H, Dokken TM, Berben SMP, Muschitiello F, Stein R, Fahl K, Menviel L,  
744 Timmermann A, Jansen E (2019) Sea ice variability in the southern Norwegian  
745 Sea during glacial Dansgaard-Oeschger climate cycles. *Science Advances* 5(3)
- 746 Sardeshmukh PD, Penland C (2015) Understanding the distinctively skewed and  
747 heavy tailed character of atmospheric and oceanic probability distributions.  
748 *Chaos: An Interdisciplinary Journal of Nonlinear Science* 25(3):036410

- 749 Sardeshmukh PD, Sura P (2009) Reconciling non-Gaussian climate statistics with  
750 linear dynamics. *Journal of Climate* 22(5):1193–1207
- 751 Schüpbach S, Fischer H, Bigler M, Erhardt T, Gfeller G, Leuenberger D, Mini O,  
752 Mulvaney R, Abram NJ, Fleet L, Frey MM, Thomas E, Svensson A, Dahl-Jensen  
753 D, Kettner E, Kjaer H, Seierstad I, Steffensen JP, Rasmussen SO, Vallelonga  
754 P, Winstrup M, Wegner A, Twarloh B, Wolff K, Schmidt K, Goto-Azuma K,  
755 Kuramoto T, Hirabayashi M, Uetake J, Zheng J, Bourgeois J, Fisher D, Zhiheng  
756 D, Xiao C, Legrand M, Spolaor A, Gabrieli J, Barbante C, Kang JH, Hur  
757 SD, Hong SB, Hwang HJ, Hong S, Hansson M, Iizuka Y, Oyabu I, Muscheler  
758 R, Adolphi F, Maselli O, McConnell J, Wolff EW (2018) Greenland records  
759 of aerosol source and atmospheric lifetime changes from the Eemian to the  
760 Holocene. *Nature Communications* 9(1):1476
- 761 Siegert S, Friedrich R, Peinke J (1998) Analysis of data sets of stochastic systems.  
762 *Physics Letters A* 243(5-6):275 – 280
- 763 Singh HA, Battisti DS, Bitz CM (2014) A heuristic model of Dansgaard-Oeschger  
764 cycles. Part I: Description, results, and sensitivity studies. *Journal of Climate*  
765 27(12):4337–4358
- 766 Stemler T, Werner JP, Benner H, Just W (2007) Stochastic modeling of experi-  
767 mental chaotic time series. *Physical Review Letters* 98(4):044102
- 768 Stommel H (1961) Thermohaline convection with two stable regimes of flow. *Tellus*  
769 13(2):224–230
- 770 Sura P, Sardeshmukh PD (2008) A global view of non-Gaussian SST variability.  
771 *Journal of Physical Oceanography* 38(3):639–647
- 772 Svensson A, Andersen KK, Bigler M, Clausen HB, Dahl-Jensen D, Davies SM,  
773 Johnsen SJ, Muscheler R, Parrenin F, Rasmussen SO, Röthlisberger R, Seierstad  
774 I, Steffensen JP, Vinther BM (2008) A 60 000 year Greenland stratigraphic ice  
775 core chronology. *Climate of the Past* 4(1):47–57
- 776 Thompson WF, Kuske RA, Monahan AH (2017) Reduced  $\alpha$ -stable dynamics for  
777 multiple time scale systems forced with correlated additive and multiplicative  
778 Gaussian white noise. *Chaos: An Interdisciplinary Journal of Nonlinear Science*  
779 27(11):113105
- 780 Timmermann A, Gildor H, Schulz M, Tziperman E (2003) Coherent resonant  
781 millennial-scale climate oscillations triggered by massive meltwater pulses. *Journal*  
782 *of Climate* 16(15):2569–2585
- 783 Venegas SA, Mysak LA (2000) Is there a dominant timescale of natural climate  
784 variability in the Arctic? *Journal of Climate* 13(19):3412–3434
- 785 Vinther BM, Clausen HB, Johnsen SJ, Rasmussen SO, Andersen KK, Buchardt  
786 SL, Dahl-Jensen D, Seierstad IK, Siggaard-Andersen ML, Steffensen JP, Svens-  
787 son A, Olsen J, Heinemeier J (2006) A synchronized dating of three Greenland  
788 ice cores throughout the Holocene. *Journal of Geophysical Research: Atmo-*  
789 *spheres* 111(D13)
- 790 Weaver AJ, Hughes TMC (1994) Rapid interglacial climate fluctuations driven by  
791 North Atlantic ocean circulation. *Nature* 367(6462):447–450
- 792 Wolff E, Chappellaz J, Blunier T, Rasmussen S, Svensson A (2010) Millennial-  
793 scale variability during the last glacial: The ice core record. *Quaternary Science*  
794 *Reviews* 29(21):2828 – 2838
- 795 Wouters J, Gottwald GA (2019a) Edgeworth expansions for slow–fast systems with  
796 finite time-scale separation. *Proceedings of the Royal Society A: Mathematical,*  
797 *Physical and Engineering Sciences* 475(2223):20180358

- 
- 798 Wouters J, Gottwald GA (2019b) Stochastic model reduction for slow-fast sys-  
799 tems with moderate time scale separation. *Multiscale Modeling & Simulation*  
800 17(4):1172–1188
- 801 Wunsch C (2006) Abrupt climate change: An alternative view. *Quaternary Re-*  
802 *search* 65(2):191 – 203
- 803 Yiou R, Fuhrer K, Meeker LD, Jouzel J, Johnsen S, Mayewski PA (1997) Paleocli-  
804 matic variability inferred from the spectral analysis of Greenland and Antarctic  
805 ice-core data. *Journal of Geophysical Research: Oceans* 102(C12):26441–26454
- 806 Zhang X, Lohmann G, Knorr G, Purcell C (2014) Abrupt glacial climate shifts  
807 controlled by ice sheet changes. *Nature* 512(7514):290–294